Timing of Triassic tectonic division and postcollisional extension in the eastern part of the Jiaodong Peninsula

Hongyuan Zhang [a,b,*], Thomas Blenkinsop[b], Zhuowei Yu[a]

a School of Earth Sciences and Mineral Resources, China University of Geosciences, No.29, Xueyuan Road, Beijing, 100083, PR China

b School of Earth and Ocean Sciences, Cardiff University, Main Building, Park Place, Cardiff, CF10 3AT, UK

Abstract

The Jiaodong Peninsula is a key region for researching the interaction between the North and South China Plates. Tectonic relationships between collision, exhumation of ultra-high-pressure (UHP) slabs, strike-slip faulting and gold mineralization, are still ambiguous. The eastern part of the Jiaodong Peninsula (Eastern Jiaodong), which includes Triassic intrusions and is less affected by the Tan-Lu Fault Zone, is a key area to examine exhumation dynamics in detail. Systematic field mapping and zircon U–Pb dating of Triassic intrusions establishes that: (1) The UHP wedge in the eastern part of the Jiaodong Peninsula can be divided into the lateral and frontal ramps of a thrust and nappe system. Dating of samples from Donglinghou (244.7±4.2 Ma) and Qingyutan (233.8±8.1 Ma) areas indicates that the collision happened at or before the Middle Triassic. (2) Postcollisional extension intrusions including the Shidao granitoid (216.2±2.4 Ma), and the Chengshantou granitoid (cut by a dolerite dyke dated at 210.5±1.0 Ma), generally strike NE and occurred in a metamorphic core complex below the Upper Jiashan-Xiangshui detachment (U-JSXS). (3) Regional faults in the Jiaodong Peninsula exploited syncollisional foliations of the UHP wedge, which resulted in faults dipping towards the NW and SE. The reactivation of the Lower Jiashan-Xiangshui shear zone (L-JSXS) and its overprinting upon the Tan-Lu fault system may have caused another major episode of exhumation of the syncollisional wedge, and could have been responsible for an extensional environment that favored gold mineralization.

Graphical abstract

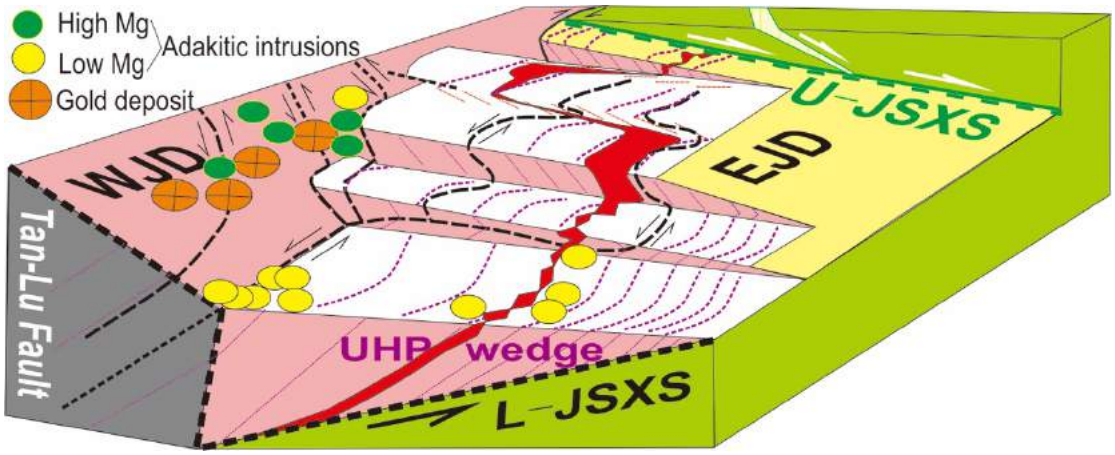

Research highlights

- Middle Triassic lateral and frontal ramps are identified in an UHP wedge.
- The Chengshantou Granite intruded along a frontal ramp in the Late Triassic.
- A Mesozoic regional shear zone was reactivated along two groups of thrust foliations.

Keywords

Eastern Jiaodong; UHP wedge; thrust system; postcollisional extension; gold mineralization.

1 Introduction

The continent of East Asia began to form due to closure of the Paleo-Tethys during the Indosinian orogeny, which includes the continent-continent collision along the Central China Orogenic Belt between the North China Plate (NCP) and the South China Plates (SCP) (Mattauer et al., 1985; Hacker et al.,1998; Oh, 2006; Wawrzenitz et al.,2006; Zhang et al.,2009; Li et al., 2017; Zhao et al., 2017; Dai et al.,2018; Yang et al.,2018). From the Middle Triassic to the Jurassic, a united continental magmatic arc appeared along the eastern coastal region of the Eurasian Plate as a consequence of the northwest oblique subduction of the oceanic Izanagi Plate (e.g. Maruyama et al., 1997). The existence of a North China plateau in the Jurassic has been challenged (Li et al., 2013), which means that two groups of Ar-Ar dating results from the Early Jurassic and the Early Cretaceous (Zhang et al., 2007a, b; Wang et al, 2014) need to be re-evaluated. From the Late Jurassic to the Early Cretaceous, there was distributed regional extension, and deep strike slip structures were locally active in Eastern North China (Liu et al., 2005; Lin et al., 2010). Variable tectonic regimes including collision, subduction, extension and strike slip faulting have dismantled the cratonic plates in three dimensions (Xu, 2006; Ge and Ma, 2014), and finally triggered extensive gold and polymetallic mineralization in the Early Cretaceous, especially the special type of giant Jiaodong gold deposit (Deng et al., 2016, 2017, 2018; Phillips and Powell, 2015; Groves et al, 2016; Goldfarb and Santosh, 2014) (Fig.1).

These events highlight the problem of the eastward continuation of the collisional

zone between the North and South China Plates. The Su-Lu Belt, an orogenic zone along the boundary of the Jiangsu Province (abbreviated as Su) and the Shandong Province (abbreviated as Lu) in Eastern China, has been displaced from the Dabie Belt by the Tan-Lu Fault Zone (Fig.1a). Some authors connect the collisional Ultra High Pressure (UHP) Belt in the Su-Lu Belt with the region between the Imjingang Belt and the Hongsung Belt (e.g. Choi et al., 2006, 2015), or with the Ogcheon Belt on the south side of the Korea Peninsula, and the Hida Belt in Northwest Japan (Yutaka et al., 2018) (Fig.1a). However, an alternative view is that the thrust zone in the Jiaodong Peninsula has been affected by the East Marginal Fault of the Yellow Sea (Zhang, 1986; Hao et al., 2007). Then the Imjingang Belt, the Hongsung Belt, and the Ogcheon Belt on the western side of the Korean Peninsula might all be located in one dextral shear zone (Cluzel et al., 1991; Oh et al., 2007, 2009; Seo et al., 2010; Oh and Lee, 2018). This shear zone has the opposite sense to shear zones and major fault zones in the Jiaodong Peninsula. According to this hypothesis, there should be Triassic evidence in the Su-Lu UHP Belt which could assist further reconstruction of the whole collisional belt.

In order to clarify the tectonic relations between the North China and South China Plates, regional geology in the collisional zone on the eastern part of the Jiaodong Peninsula is studied in detail. New subunits are divided according to collision related thrust and strike-slip shear zones. The tectonic significance of Triassic intrusions in these units is discussed from outcrop, hand specimen and microstructural evidence. Several new U-Pb dates from these intrusions are discussed and classified with respect

to the collision and postcollisional extension.

2 Regional geology and new tectonic division

The Eastern Jiaodong region is situated at the eastern part of the Su-Lu Orogenic Belt (Fig.1b), and includes an ophiolite mélange zone (Fig. 1; Wang et al., 1995; Lai, 1997; Ni, 1999). To the west of the ophiolite zone, rocks including high pressure granulite metamorphic rocks in the west of Weihai were inferred to represent the Jiaodong Group of the lower crust of the North China Plate (Wang et al., 1995). Also to the west, in the Yantai region, there is a metamorphic cover unit containing marbles and quartzites (the Fenzishan Group). To the southeast of the mélange belt, the Jiaonan Group, possibly formed in the Triassic, occurs in a region of strongly foliated gneiss extending to the Yellow Sea, including many UHP metamorphosed eclogite lenses containing zircons with a Neoproterozoic core-Late Triassic mantle microstructure (Yang et al., 2002, 2003, 2009).

Traditionally, the Jiaodong Group is considered as an Archean sedimentary basement and the overlying Fenzishan Group is unconformable, indicating that the Jiaodong Movement occurred between late Neo-Archean and early Paleo-proterozoic (Zhu and Xu, 1994). The Fenzishan Group might have experienced one later tectonic event between the Paleo- and Meso-proterozoic ("the Fenzishan Event", Zhu and Xu, 1994), which was simultaneous with the Lvliang Movement in Central North China. The Jiaonan Group is also considered as an Archean sedimentary basement which is

structurally divided from the Jiaodong Group by the Wulian fault (SBGMR,1991) or a possible ophiolite mélange zone (Fig. 1). Protoliths of the Jiaonan Group are inferred to be mainly bathyal volcanic rocks and marine sedimentary rocks (SBGMR,1991; Wang et al., 1995; Lai, 1997; Ni, 1999). Later studies further recognized some smaller Paleo-proterozoic cover units over the Jiaonan Group which have a similar age but a different tectonic background to the Fenzishan Group (Song and Miao, 2003).

The South China Plate is in contact with the Jiaonan Group (or the Su-Lu Orogen) along the Jiashan-Xiangshui shear zone (JSXS). The South China Plate experienced a folding and thrusting event in the Nanxiang Movement in the Middle Triassic (Ge, 1987; Ge et al., 2014). Study of the Triassic magmatic units in the southeastern coastal zone of the Jiaodong Peninsula (Guo et al., 2005) suggests that these units are related to decratonization in the eastern North China Plate (Yang and Wu, 2009) (Table 1). The existence of the JSXS south of the Triassic magmatic zone and below the Yellow Sea has been inferred by studies of Bouguer gravity and aeromagnetic anomalies in the south coastal region of the Shandong Peninsula. The JSXS has been considered as the boundary zone of the Su-Lu Orogen and the South China Plate (Zhang et al., 2017a,b).

The Jiadong Peninsula can be divided into three units: the North China Plate (I), the orogenic belt (II) and the South China Plate (III) (Fig. 2). The orogenic belt (II) can be divided into the ophiolite mélange zone (II-1) and the eclogite-rich ductile thrust shear zone (II-2) according to the above regional geological review. Below, new divisions of the eclogite-rich unit (II-2) are proposed based on structural features of the

collision related regional thrust and nappe system.

The eclogite-rich unit (II-2) can be considered as a belt of ductile shear zones surrounding metamorphic blocks. The orientation of fabrics and the kinematics of the Triassic shear zones allow a new subdivision of unit II-2: In the southwest is an Early-Middle Triassic thrust-sense shear zone, unit II-2-①; In the middle region is a SSE-SE trending Early-Middle Triassic sinistral-oblique slip shear zone, unit II-2-②; To the northeast of II-2-② is unit II-2-③, a folded block divided into two parts by the Lidao Fault Zone (LDFZ).

Structural elements show overprinting relations (Fig. 3), especially in the Puwan region (Fig. 4). The stereoplots show three different stages of structural elements in this area. Foliations and lineations of the first stage (D_1) caused by the contractional event during orogeny are plotted in red as S_1 and L_{1a}, respectively. Basic and granitic dykes, and veins (shown in green), were mainly formed later, in the Late Triassic extension stage (D_2). Overprinting joints and quartz veins were formed in a strike-slip stage (D_3) and (shown in black). To the east of the north part of the gneissic ophiolite zone (II-1) and north of the Weideshan granitoid (WDSG), unit II-2-② is a shear zone which has ductile sinistral-oblique slip kinematics according to the relations between S_1 and L_{1a} (most of which are gneissic foliations with extensional lineations). Foliations in unit II-2-② generally trend SE-SSE. This is different from those of unit II-2-①, south of the WDSG, with foliations trending NE-ENE. In the Puwan-Doushan-Mage area, structural style changes abruptly into a folded region near the Haixitou area, indicating the

existence of boundary between units II-2-② and II-2-③. Both units II-2-① and II-2-③ contain fold hinges with low plunges indicating that similar deformation occurred during the Early-Middle Triassic thrusting event before they were intruded by plutons in the Late Triassic.

There are nearly constant paleostress values in unit II-2-①, but quite variable strain values, which reduce from rims of the Shidao Granite towards the northwest (Fig.2; Zhang, 2003; Zhang et al., 2005). Total shortening of UHP rocks was estimated as more than 100 km (Ye and Cong, 2000). The total displacement of the ductile shear zone in Eastern Jiaodong has been estimated as about 117 km according to the decreasing trend of shear strain values along a profile from Moyedao to Datuan (Zhang, 2003; Fig. 2). Considering that the average lineation orientation (trend/plunge) is about 170º/30º and the average strike of foliation is about 65º, the angle between the average stretching lineation and the average strike of foliation is about 77º. Therefore, the sinistral strike slip and reverse components of displacement are about 26 km and 114 km, respectively ($S_{\text{slip}} = 117 \times Cos77 \approx 26km$; $S_{thrust} = 117 \times Sin77 \approx 114km$).

3 Samples from intrusions in the Jiaonan Ductile Shear Zones

Intrusions can constrain the time of regional contraction and postcollisional extension. This section focuses on the structural characteristics of the granitoids developed in the Rongcheng region, southeast of the ophiolite mélange. The granite

samples come chiefly from granitic bodies, dykes or sills. Figure 2 shows four new sample locations in Eastern Jiaodong. Since the axes of the Chengshantou granitoid (CSTG) and the Triassic Shidao granitoid (SDG) are parallel to the strike of the ductile shear zone, it was hypothesized that they should have same intrusion age, although previous work classified the CSTG as a Cretaceous granitoid (National geological maps with scales of both 1:200,000 and 1:500,000, e.g. Wu et al., 2017; Deng et al., 2018). Whether granitic branches intruding the gneiss zone with UHP rocks showed similar ages was also investigated.

Intrusions were selected from each unit to determine the minimum age of the syncollisional thrust system and the time of postcollisional extension. Two specimens were sampled from unit II-2-① (Fig. 2), including one from the Shidao granitoid (SDG in Fig. 2), sample (140304) in the south coastal region, and one gabbroic sample (140203 from Donglinghou) in foliated rocks in the north of the unit. One specimen was sampled from unit II-2-②, sample (140302) from the Qingyutan granite sill in the eastern coastal of Rongcheng. One dyke sample from the Chengshantou granitoid (CSTG) (131102) was obtained in unit Ⅱ-2-③. According to the field relations of these intrusions, the sill samples (140203, 140302) should represent the minimum (latest) time of movement along the foliations from the syncollisional thrust system, while the two granitoid or dyke samples (140304, 131102) should be later than the Triassic thrust system.

184 **3.1 Samples of thrust-related intrusions**

185 **3.1.1 Gabbro sill sample (140203) from Donglinghou village**

186 140203 is sampled from a gabbro sill with thickness of 1.5-2 m which intruded
187 foliated gneiss host in a highway profile near Donglinghou Village (Fig. 2; Fig. 5A).
188 The location is at the north part of the unit II-2-①.

189 The boundary of the intrusion is parallel to the host rock foliation (Fig. 5A).
190 Foliation orientation data of the host rock in the profile and adjacent areas are plotted
191 in Fig. 5B. Gneiss from the host was faulted into the gabbro during horizontal
192 shortening and vertical lengthening.

193 A few quartz veins can be found in cracks in the gabbro sill, possibly indicating a
194 later sinistral shearing event in the Early Jurassic (Fig. 5A-B). One quartz vein sample
195 yielded a gold content of 4.76 μg/g. The gold is observed inside fractured pyrite of the
196 deformed quartz veins (Fig. 5B-C). Since retrograde metamorphism may have
197 affected the surrounding area of the quartz veins and cracks, 140203 is selected from
198 the less deformed part in the center of larger gabbroic blocks, 3-5 centimeters away
199 from a dense crack zone (Fig. 5B).

200 The fine grained gabbro sample is mainly composed of retrograded pyroxene (～
201 25%), plagioclase (～35%), hornblende (～35%) and other minerals (e.g. quartz,
202 pyrite, ～5%) (Fig. 5D).

3.1.2 Gneissic granite sample (140302) from Qingyutan

140302 is sampled from a gneissic granite intrusion along foliations of the gneissic host in the Qingyutan coastal area to the east of Rongcheng City (Fig. 2). Foliations with mineral elongation lineations were developed extensively in host rocks (S1-Foliation (dip direction/dip): 075º/82º; L_1-Lineation (trend/plunge): 355º/35º) (Fig.3a, Fig. 5G-H).

The fine grained granite sample is mainly composed of quartz (fine grains with some undulose extinction, ～ 35%), K-feldspar (partly fine grained and recrystallized, ～30%), plagioclase (with mechanical twinning, ～30%), biotite and opaque minerals such as pyrite (～5%) (Fig. 5I-J). According to the microstructural features and the intrusion relations with the host foliations, the crystallization age of magmatic zircons from this sample represent will represent the minimum time of the latest movement.

3.2 Postcollisional extension intrusions

3.2.1 Dolerite dyke sample (131102) from CSTG

A dyke specimen intruding the Chengshantou granitoid (CSTG), 131102, was obtained from a granitoid outcrop southwest of Luofenggang, Chengshan Horn (Fig. 2; Fig. 6AB). There is little indication of deformation from thin section. This fine grained dolerite is composed of plagioclase (60%), pyroxene (30%), chlorite (5%) and some accessory minerals (5%) (Fig. 6C).

The CSTG granite is traditionally considered as a Cretaceous intrusion. However it has proven hard to obtain good zircon dating results, since metamorphic zircons that experienced UHP metamorphism in host gneiss rocks can be easily carried into magma during intrusion of the Chengshantou granite. The dyke sample is intended to constrain the timing of CSTG intrusion.

3.2.2 Porphyry granitic dyke sample (140304) from SDG

A specimen of the Shidao granitoid (SDG), 140304, was obtained from a dyke in the east of the Shangtanjia Village to the east of Chishan Town (Fig.2). The location is within the boundary zone of the SDG. With an orientation of 060º/89º, the dyke (S_2) intruded into gneissic rocks (S_1) (Fig. 6F). In the outcrop, it is also clear that a set of sinistral fractures (S_3) deformed the host gneiss rocks. Sample 140304 is from the little deformed region some distance from the S_3 zone. Microscopic deformation in section of 140304 is limited. A porphyritic texture can be clearly observed (Fig. 6G).

The mineral composition includes plagioclase (fine grained in matrix area, ～40%), potassium feldspar (hypidiomorphic phenocrysts, ～20%), quartz (banded with fine crystallization, ～30%), biotite (phenocrysts, ～5%) and other minerals (～5%). With very few deformation structures observed in sample 140304, the zircon date should represent the timing of intrusion.

4 Experimental methods and result

4.1 Experimental methods

The separation of zircon was completed by the conventional crushing, separation, magnetic and gravity liquid separation, and final selection under the binocular microscope. While making the samples, a test zircon was placed on a glass and fixed with a colorless transparent epoxy resin, then after the resin cured fully, the zircon was coarsely and finely ground until the zircon center was exposed and then polished. After taking reflected light and transmitted light photos of the zircon samples, we analyzed the image with cathodoluminescence (CL) using the scanning electron microscope, and then cleaned and gold-plated the sample. Cathodoluminescence image analysis confirmed the type of the zircon, and the point to analyze was chosen. Larger idiomorphic zircons were selected, and zircons with crack and inclusions were avoided as far as possible.

The zircon U-Pb isotope geochronology of three samples (140203, 140302, 140304) was completed by the LA-ICP-MS microanalysis laboratory in the State Key Laboratory of Geological Processes and Mineral Resources, China University of Geosciences, Beijing: the laser ablation system is the Geolas 193 excimer solid sample system of the Coherent company, US. The ICP-MS is the X Series 2 type quadrupole plasma mass spectrum of the Thermo Fisher company, US. Testing conditions include that the diameter of the laser spot beam is 32μm, the frequency is 6 Hz, the carrier gas

is He and the compensation gas is Ar. The US national standard reference materials NIST610 was used to optimize the instruments and taken as the external standard for determination of the trace element content. The standard zircon 91500 (Wiedenbeck et al, 1995, 2004) was used as the external standard of dating, and the standard zircon GJ-1 as the monitoring sample. In the process of sample testing, we measured the standard zircon 91500 twice every five sample points. The signal acquisition time of each point was 100 s, the top 20 s was the background signal acquisition time, and the sample signal acquisition time is 50 s. After the test was completed, we used the software ICPMSDataCal (Liu et al., 2008) to process the test data and finish the age calculation, and graphs were drawn with the ISOPLOT 4.15 software.

The zircon U-Pb isotope geochronology of one sample (131102) was carried out by a laser ablation inductively coupled plasma mass spectrometer (LA–ICP–MS) at the Geological Laboratory Center of the Tianjin Institute of Geology and Mineral Resources. Similar testing procedures of that in CUGB were completed, including the use of standard zircon 91500 and point selections from zircons in the sample. Concordia and weighted average plots were finally processed by the software referred to above.

4.2 Geochronological Results

The samples either contain mixtures of magmatic and inherited zircon, or only magmatic zircons.

4.2.1 Samples of thrust-related intrusions

Samples 140203 (Donglinghou, Fig.5A-F) and 140302 (Qingyutan, Fig.5G-L) from smaller intrusions in UHP gneissic rocks show a mixture of magmatic and inherited zircon.

Zircons from sample 140203 (Donglinghou) are mainly idiomorphic or hypidiomorphic crystals, with average sizes ranging from 70 to 180μm in diameter, and the aspect ratios between length and width are from 1:1 to 4:1 (Fig. 5E). The zircon cores are usually in dark color and are interpreted as inherited parts of zircons (Corfu et al., 2003; Wu and Zheng, 2004). The narrow edge of the zircon is often bright and relatively white representing the new growth. The wider edge can be dated to obtain the crystallization time because of the igneous texture of the overgrowth. Inherited parts of zircons in 140203 mainly formed in the Paleoproterozoic Statherian Period (about 1800 Ma), while the rim parts of zircons mainly formed between 255-235 Ma, typically in the Ladinian (Middle Triassic) Epoch (Fig. 5E).

Zircons from the sample 140302 (Qingyutan) are also mainly hypidiomorphic crystals with round to angular edges, with average sizes ranging from 70 to 300 μm in diameter, and aspect ratios from 1:1 to 3:1 (Fig. 5K). The zircon cores are usually dark and sometimes show oscillation texture, and are interpreted as inherited parts of zircons (Corfu et al., 2003; Wu and Zheng, 2004). The zircon edges of sample 140302 are wider than those of 140203 (gabbro sill sample from Donglinghou). Inherited parts of zircons in 140302 mainly formed between 811-597 Ma in the Neoproterozoic Era, while the

rims of zircons mainly formed between 250-226 Ma with typical ages between the Anisian and Carnian in the Middle Triassic (Fig.5L).

The concordia and weighted average plots of the Donglinghou sample (140203) show two grouped mean values, 244.7±4.2 Ma for magmatic rims of zircons and 1779±20 Ma for cores (Fig.5F; Table 2 and Table 3). The concordia and weighted average plots of the Qingyutan sample (140302) also show two very concentrated mean values, 233.8±8.1 Ma for magmatic rims of zircons and 724.6±8.3 Ma for cores (Fig.5L; Table 2 and Table 3). Dates of the zircon rims are similar for the two samples. It is hard for gabbroic or granitic intrusions to form zircons in hosts of UHP metamorphosed rocks, so the dated zircon edges should have formed when the gabbro intruded rather than being inherited zircons.

4.2.2 Postcollisional extension intrusions

Samples 131102 (CSTG, Fig. 6AB) and 140304 (SDG, Dyke, Fig. 6F) show mainly magmatic zircons. Zircons obtained from sample 131102 are transparent, translucent or colorless, with grain diameters ranging from 50 to 250 μm and aspect ratios from 1:1 to 5:1. Cathodoluminescence (CL) images show that zircon crystals have the vibration ring band and are magmatic, indicating newly formed zircons by dolerite intrusion into the granitoid host of the CSTG. This is consistent with previous discussion on Triassic magmatic zircons (Liu et al., 2009a). In sample 140304, the zircons are translucent, the grain diameter ranges from 50 to 200 μm, and the aspect ratio is from 1.2:1 to 2.8:1. Cathodoluminescence (CL) images reveal that zircon

crystals have the vibration band of magmatic zircon.

The granitoid and minor intrusions represented by these samples are all products of the Norian magmatic events in the Late Triassic (Table 2 and Table 3). A weighted average age of the dolerite dyke in Chengshantou Granite (CSTG) is 210.5±1.0 Ma (131102, Fig. 6E, Table 2). The age data is very grouped and prove that the CSTG is Late Triassic rather than Cretaceous. A weighted average age of the sample from the Shidao Granite (SDG) is 216.2±2.4 Ma (140304, Fig. 6I, Table 2) which is similar to previous results from granitoids in unit II-2-① (Table 1; Yang et al., 2002; Chen et al, 2003; Yang et al, 2005; Guo J.H.et al., 2005; Tang J.et al., 2005; Xu et al.,2006; Liu， 2009b).

5 Discussion

Thrust and sinistral shear zones are the main tectonic features in the Jiaodong region. The initial relations of the two structural features and how they relate to each other during collision are important questions for understanding the Late Triassic magmatism and extension. Mesozoic postcollisional extension with granitic domes was proposed by Faure et al. (1996) within South China Plate. But to investigate the relations between the postcollisional intrusions and their previous structures, it is more straight forward to make observations at boundaries than within plates.

5.1 Nature of shear zones between the UHP wedge and South China Plate in the eastern part of the Su-Lu Orogeny

Foliation in Eastern Jiaodong, the eastern part of the Su-Lu Orogen, generally dips in the opposite direction to foliation in the western part of the Su-Lu orogeny, the Lianyungang area. In the Lianyungang area, foliation mostly dips to the north (Zheng et al.,2005; Tang et al., 2006), while in the Eastern Jiaodong, foliation usually dips to the southeast with higher values (60-80°) (Fig.7). This may indicate that there were lateral ramps during thrusting and folding in these two sections in the Triassic orogeny. However, a typical geophysical velocity profile crossing the Su-Lu orogeny and between the east and west parts, shows a crocodile mouth like or wedge-shaped structure (Xu et al., 2002; Kun et al., 2018). Therefore, it is possible that the top to the north thrust structures caused by the contraction between UHP terrane and overthrusting of the upper crust of the South China Plate are preserved, while in the western section of the Su-Lu Orogen or in the Lianyungang region, there is no obvious residue of the upper crust of the South China Plate.

According to the above discussion, there should be evidence of two boundaries between the UHP terrane and the South China Plate: the Upper Jiashan-Xiangshui Shear Zone (U. JSXS) and the Lower Jiashan-Xiangshui Shear Zone (Fig.1). The upper and lower surfaces in this collisional syntaxis with crocodile mouth geometry may have been reactivated and became two detachments, an earlier upper one and a later lower one. This is comparable to the syntaxis region of the Eastern Himalaya, to the east of

361 the Sagaing Fault and the Main Central Thrust, which is likely to have a similar
362 crocodile mouth geometry (SoeThura and Watkinson, 2017). The Jiashan-Xiangshui
363 Shear Zone (JSXS), being cut by the Tan-Lu Fault Zone in the southwest and extending
364 to the Yellow Sea, is usually considered as the north boundary of the Yangtze Plate on
365 the basis of aeromagnetic and gravity anomalies (Xiao Q.B., 2008; Zhang et al.
366 2017a,b).

367 According to section 2 above, in Eastern Jiaodong the UHP wedge unit (II-2) can
368 be divided into three units, II-2-①, II-2-② and II-2-③ (Figs.2-4). Unit II-2-② can
369 be interpreted as a ductile sinistral lateral ramp of the Su-Lu syncollisional regional
370 thrust and nappe system, and there are several similar ramps with deep ductile dextral
371 shear zones in the Southwestern Korean Peninsula (Fig.1). Units II-2-① and II-2-③
372 are frontal ramps with evidence of thrusting (Figs.3, 4).

373 ## 5.2 Timing of the lateral ramp

374 The dyke or sill samples (140302, 140203) within unit II-2-② and the north
375 eastern part of the unit II-2-① should give the minimum age of the lateral ramp shear
376 zone from outcrop relations between intrusions and ramp foliations (S_1) and lineations
377 (S_L) (Fig. 3a, Fig. 5). The shear zone formed before the Middle Triassic according to
378 the zircon crystallization ages of 240 Ma in these samples. This earlier set of intrusions
379 in the Middle Triassic may also represent the minimum formation time of frontal ramps
380 of the regional syncollisional thrust and nappe system (Fig.3c).

381 The thrust and nappe system deformed the UHP-wedge in the Middle Triassic
382 during collisional orogenesis between the North China Plate and the South China Plate.
383 According to Wan (2011), sinistral displacement on the Tan-Lu Fault Zone (Fig. 1) was
384 about 150-200 km in the Middle-Late Triassic. Initiated from the Triassic deep ductile
385 sinistral ramps inside the Dabie-Su-Lu Orogeny, the Tan-Lu Fault Zone caused much
386 larger displacement and exhumation in its neighboring region than more distant places.
387 An example of a larger displacement profile is the one crossing the Lianyungang
388 Region, in the southwestern section of the Su-Lu Orogen (e.g. Zheng et al., 2005; Ye et
389 al., 2009).

390 It is interesting that the intrusions in the thrust system of Eastern Jiaodong were
391 simultaneous with the Hida granite in Japan and the Cheongsan Granite in South Korea
392 (e.g. Yutaka et al., 2018). These intrusions were all emplaced along ductile shear zones
393 (Cluzel et al., 1991; Oh et al., 2007; 2009; Seo et al., 2010; Oh and Lee, 2018) (Fig.1a).
394 Located in the same regional contraction zone between the southeastern North China
395 Plate and along the northeastern boundary of the South China Plate, these three belts
396 experienced Early-Middle Triassic Orogeny, Late Triassic postcollisional extension and
397 a Jurassic-Cretaceous strike-slip event (Table 4). When making reconstructions in the
398 three regions, it is important to consider the geometry of the UHP wedge between two
399 plates.

5.3 Significance of the NE striking intrusions in the Rongcheng Region

Most dating from different parts of the Shidao Granite (SDG) in unit II-2-① proves the existence of voluminous Late Triassic magmatism (Tables 1, 2). The Chengshantou Granite (CSTG) II-2-③ also formed in the Late Triassic according to our results from the intruded dyke.

Tectonically, the Eastern Jiaodong granitoids should occur in the UHP prism near the tip line between the SCP and NCP (Fig.1b; Fig.7a) which is caused by the detachment between the UHP wedge and the top of the SCP. This intrusion process can be considered as postcollisional extension (e.g. Fossen and Rykkelid, 1992). The existence of the Jiashan-Xiangshui fault zone (JSXS), which currently emerges below the South Yellow Sea, can be demonstrated by aeromagnetic evidence (Xiao Q.B., 2008; Zhang et al. 2017a,b). The Jiashan-Xiangshui fault zone may play the role of a detachment below the upper crust of the SCP that governed the exhumation of the UHP wedge in the Su-Lu Region (Fig.1b and section A-A'; Fig.7c). According to gravity and aeromagnetic studies (Choi et al., 2006; 2015), the Late Triassic granitoids (including CSTG and SDG) are on the Qianliyan Uplift (the east extended Jiaodong Peninsula). The Qianliyan uplift possibly contains the same structures before intrusion as those in the Eastern Jiaodong region, i.e. the frontal ramp of the thrust and nappe regime before the Middle Triassic.

Regional relations of structural elements may reflect the distance from the detachment. There is a subparallel relation between strikes of S_1 foliations and the trend

of SDG in unit II-2-①. Strikes of S_1 foliations with dykes at point Wh1325 are also sub-parallel to the trend of CSTG in unit II-2-③ (Fig. 4). However, strikes of dykes at points Wh1323, 1324, 1327, 1328 in the north of the unit II-2-② all show large oblique angles to S_1 foliations (Fig.4), indicating a greater distance from the detachment.

There were two Mesozoic extension events, in the Late Triassic and Early Cretaceous, deduced both from the Tan-Lu Fault Zone and the Dabie-Su-Lu Orogenic Belt in the Mesozoic (Zhang et al., 2002; Zheng et al., 2005; Yan et al., 2018). The Late Triassic magmatism represented by CSTG and SDG should have intruded across the UHP wedge but below the top detachment of the UHP wedge, the upper Jiashan-Xiangshui Shear Zone (U. JSXS) during postcollisional extension (Fig.7c).

5.4 Mesozoic structural features after the Triassic

Our dating suggests the minimum time of the collisional related regional thrust and nappe system and the time of postcollisional extension. The collisional related regional thrust and nappe system has been intruded by several episodes, including three stages of granitic intrusions, and followed by wedge emplacement (Late Triassic, Late Jurassic, Early Cretaceous). It is important to exclude the effects of later structures.

Several NE-NNE trending sinistral strike-slip shear zones activated in the Early Jurassic have been mapped in Unit II-2-① (Fig.2). These shear zones overprinted the previous Triassic thrust system in the UHP-wedge. According to the regional relations, Late Jurassic intrusions such as the Wendeng Granite (WDG) intruded along such NE-

441 NNE trending shear zones, indicating reactivation of the Triassic thrust system in the
442 UHP wedge. Published Early Jurassic Ar-Ar ages from near Dashijia to the south of the
443 WDG (Hornblende in mylonite, ～190 Ma, Zhang et al., 2007b) could demonstrate
444 reactivation along the boundary region between units II-1 and II-2-①.

445 Jurassic-Cretaceous faults formed after the intrusion of the Jurassic Wendeng
446 granitoid (WDG), e.g. the LDFZ, RCFZ and SDFZ (shown as D_3 in Figs. 2-4),
447 especially along boundary zones of the above units, indicating a similar sinistral strike-
448 slip related emplacement processes including local pull apart structures with granitic
449 intrusions and basin sedimentation. The distribution of these fault zones is more
450 localized than the Triassic and Early Jurassic shear zones. Fault zones in this stage,
451 shown in black lines in Fig. 2, were active at about ～125 Ma and around the intrusion
452 time of the Weideshan granitoid (WDSG) and the time of eruption of volcanic rocks
453 and deposition of sedimentary rocks in Cretaceous basins (Zhang et al., 2007b).

454 The Early Jurassic Ar-Ar date indicates that the UHP wedge in Eastern Jiaodong
455 has an earlier emplacement with a comparatively smaller movement during late
456 Mesozoic (Fig. 7d). Both Early Jurassic Ar-Ar dates (200-180 Ma) in the research area
457 (Zhang et al. 2007b) and similar results published in Dabie Mountain (Wang F. et al.,
458 2014; Yang et al.,2014) indicate the same reactivation and emplacement event along
459 boundaries of former units in these places, which had similar later tectonic processes to
460 the UHP wedge after the Indosinian Orogeny and postcollisional extension.

461 Another piece of evidence that might prove the emplacement of the UHP wedge

462 is the observation that in the southwestern and northwest side of the Jiaodong Peninsula
463 there are two types of Early Cretaceous adakitic rocks shown according to Gu et al.
464 (2013) in Fig. 1, but neither type is found from the Eastern Jiaodong region (although
465 there are some major granitic intrusions in this period, e.g. the Late Jurassic Wendeng
466 (WDG) and the Early Cretaceous Weideshan (WDSG) granitoids). The source of the
467 low-Mg adakitic rocks could be the lower crust of the South China Plate below the
468 Lower Jiashan-Xiangshui Shear Zone (L. JSXS) (Figs.7d). That could mean the UHP
469 wedge was preserved more completely in Eastern Jiaodong than in Western Jiaodong
470 (Lianyungang-Qingdao section) during the period after postcollisional extension and
471 before intrusion of the adakitic rocks (Fig.7d).

472 ## 5.5 Gold mineralization in the research region

473 The 3D models shown by Fig.7 explain why the shear zones in Western Jiaodong
474 (WJD) dip NW while those in Eastern Jiaodong (EJD) dip SE. The occurrences of the
475 main shear zones were strongly affected by two groups of syncollisional foliations in
476 the UHP wedge. The foliations in the lower half of the UHP wedge mainly dip NW to
477 -N, while those in the upper half region of the UHP wedge dip SE to -S. The simplified
478 2D models shown by Fig.8 show a possible mechanism for Jiaodong gold deposit
479 formation that relates to structures of the syncollisional Su-Lu UHP wedge.

480 Some gold mineralization in the southwestern part of the research region was
481 mapped (Liu et al., 1994) in the top half of the wedge and the UHP Belt (Fig.7d). This
482 mineralization style is similar to the gold bearing quartz vein inside the gabbro sill near

Donglinghou (Fig.2a; Fig.5C). This vein formed in a sinistral shearing event (D_3) after the gabbro intrusion, possibly in the Early Jurassic before the intrusion of the Wendeng granitoid (WDG, Fig.2).

However, the major gold mineralization in the whole Jiaodong Peninsula occurred in the Early Cretaceous (Deng et al., 2018; Phillips and Powell, 2015; Groves et al, 2016; Goldfarb and Santosh, 2014), which was later than the gold mineralization in the research region discussed above. Distribution of those Cretaceous world-class to Giant disseminated/microbreccia and vein-type gold deposits is governed by NNE-trending regional faults in an E-W-trending corridor (Fig.1; Deng et al., 2018).

Considering the major Cretaceous basins, NNE-trending faults, and locations of gold mineralization together with the Triassic orogeny and postcollisional extension, a new tectonic model can be set up (Fig. 8). Most regional faults, belonging to the Tan-Lu fault system, were parallel to syncollisional foliations in the North China wedge (including the Su-Lu UHP wedge, Fig. 8a). The wedge first experienced a Late Triassic emplacement during movement of the Upper Jiashan-Xiangshui Detachment (U-JSXS; Fig. 8b), and then sinistral shear related to the Tan-Lu fault system (Fig. 8c). A further exhumation occurred with the development of the Tan-Lu fault system in the Early-Middle Triassic, which was caused by a regional extensional environment possibly governed by the L-JSXS detachment (Fig. 8d).

Extensional structures that controlled the Cretaceous gold deposits might be one part of the L-JSXS detachment system, a previous contractional boundary between the

UHP wedge and the lower crust of the South China Plate. The dynamic force for extension could come from magmatic activities (e.g. dykes, Liu et al., 2018) below the detachment. In general, the large-scale gold deposits in the northwest of Jiaodong are located in the middle and lower part of the wedge and in a region of larger magnitude exhumation near the Tan-Lu fault (e.g. Zhang et al., 2019). Minor gold mineralization in Eastern Jiaodong formed in the Jurassic in the upper part of the wedge and in the UHP zone.

6 Conclusion

(1) The UHP wedge in Eastern Jiaodong can be divided into the lateral and frontal ramps of a thrust and nappe system during collisional orogeny. Dating of the Donglinghou gabbro (244.7±4.2 Ma) and Qingyutan gneissic granite (233.8±8.1 Ma) indicates that this event happened at or before the Middle Triassic (Anisian, Ladinian, Early Carnian).

(2) Intrusions relating to postcollisional extension, including the Shidao granitoid (SDG, 216.2±2.4 Ma), and the Chengshantou granitoid (dolerite dyke intruding the CSTG, 210.5±1.0 Ma), generally strike NE. The Upper Jiashan-Xiangshui detachment (U-JSXS) is thought to be reactivated on top of the metamorphic core complex with Late Triassic intrusions. After the Triassic, the Lower Jiashan-Xiangshui Shear Zone may have been reactivated.

(3) Major regional Mesozoic faults in Jiaodong Peninsula occurred parallel to the

syncollisional foliations of the UHP wedge. The overprinting Lower Jiashan-Xiangshui detachment system might govern the extensional environment, creating favorable conditions for gold mineralization in the Cretaceous. The geometry of the UHP wedge between two plates should be considered seriously when making reconstructions in Sulu, South Korea and Japan.

Acknowledgement

The research has been supported by several academic projects since 2000, such as the National Natural Science Fund project (No.41230311 and No.41430211), the Public Welfare project from the Ministry of Land and Resources (No.201211024-04) and projects from China Geological Survey (12120114014401, 1212011121188). The authors are sincerely grateful to the following professors for their help in different stages: Jun Deng and Junlai Liu from China University of Geosciences, Jinlong Ni from Shandong University of Science and Technology, Quanlin Hou from University of Chinese Academy Sciences and Zongqi Wang from Chinese Academy of Geological Sciences. We also thank some students including Wei Chen, Zhenhui Ma and Jinsheng Wang for their accompanying field survey or laboratory tests. The first author of this paper is an academic visitor supervised by Professor Christopher J. MacLeod in Cardiff University and supported by China Scholarship Council. We also thank some colleagues from Cardiff University, such as Dr Marc-Alban Millet, Dr James Lambert-Smith, Dr Adam Beall, Dr Katie McFall, Dr Matthew Price and Dr Jack Williams for

their suggestions on related problems. Professor Yunpeng Dong, Professor M. Santosh and five anonymous reviewers are specially thanked for their valuable comments and suggestions during the revision process.

References

Chen, J.F., Xie, Z., Li, H.M., Zhang, X.D., Zhou, T.X., Park, Y.S., Ahn, K.S., Chen, D.G., Zhang, X., 2003. U-Pb zircon ages for a collision-related K-rich complex at Shidao in the Sulu ultrahigh pressure terrane, China. Geochemical Journal 37, 35-46.

Choi, S., Oh, C.W., Luehr, H., 2006. Tectonic relation between northeastern China and the Korean peninsula revealed by interpretation of GRACE satellite gravity data. Gondwana Research 9, 62-67.

Choi, S., Ryu, I.C.， Götze, H.J., 2015. Depth distribution of the sedimentary basin and Moho undulation in the Yellow Sea, NE Asia interpreted by using satellite-derived gravity field. Geophysical Journal International 202, 41-53.

Cluzel, D., Lee, B.J., Cadet, J.P., 1991. Indosinian dextral ductile fault system and synkinematic plutonism in the southwest of the Ogcheon belt (South Korea). Tectonophysics 194, 131-151.

Corfu, F., Hanchar, J.M., Hoskin, P.W.O., Kinny, P., 2003. Atlas of zircon textures. Reviews in Mineralogy and Geochemistry 53, 469-500.

Dai, L., Li, S., Li, Z.-H., Somerville, I., Suo, Y., Liu, X., Gerya, T., Santosh, M., 2018. Dynamics of exhumation and deformation of HP-UHP orogens in double subduction-collision systems: Numerical modeling and implications for the Western Dabie Orogen. Earth-Science Reviews 182, 68-84.

Deng, J., Wang, Q.F., 2016. Gold mineralization in China: Metallogenic provinces, deposit types and tectonic framework. Gondwana Research 36, 219-274.

Deng, J., Wang, Q.F., Li, G.J., 2017. Tectonic evolution, superimposed orogeny, and composite metallogenic system in China. Gondwana Research 50, 216-266.

567 Deng, J., Yang, L.Q., Li, R.H., Groves, D.I., Santosh, M., Wang, Z.L., Sai, S.X., Wang, S.R., 2018.
568 Regional structural control on the distribution of world-class gold deposits: An overview from the
569 Giant Jiaodong Gold Province, China. Geological Journal, 1-14.
570 Faure, M., Sun, Y., Shu, L., Monié, P., Charvet, J., 1996. Extensional tectonics within a subduction-type
571 orogen. The case study of the Wugongshan dome (Jiangxi Province, southeastern China).
572 Tectonophysics 263, 77-106.
573 Fossen, H., Rykkelid, E., 1992. Postcollisional extension of the Caledonide orogen in Scandinavia:
574 Structural expressions and tectonic significance. Geology 20, 737-740.
575 Gao, Y., Mao, J.W., Ye, H.S., Li, Y.F., 2018. Origins of ore-forming fluid and material of the quartz–vein
576 type Mo deposits in the East Qinling–Dabie molybdenum belt: A case study of the Qianfanling Mo
577 deposit. Journal of Geochemical Exploration 185, 52-63.
578 Ge, X.H., 1987. Nappe structures in the Ningzhen mountains. Journal of Changchun College of Geology
579 17, 143-154 (In Chinese with English abstract).
580 Ge, X.H., Ma W.P., 2014. A Course of China Regional Geotectonics. Beijing: Geological Publishing
581 House, pp.1-466 (In Chinese).
582 Goldfarb, R.J., Santosh, M., 2014. The dilemma of the Jiaodong gold deposits: Are they unique?
583 Geoscience Frontiers 5 (Issue 2), 139-153.
584 Groves, D.I., Santosh, M., 2016. The giant Jiaodong gold province: The key to a unified model for
585 orogenic gold deposits? Geoscience Frontiers 7 (Issue 3), 409-417.
586 Guo, J.H., Chen, F.K., Zhang, X.M., Siebel, W., Zhai, M.G., 2005. Evolution of syn- to post- collisional
587 magmatism from north Sulu UHP belt, eastern China: zircon U-Pb geoehronology. Acta Petrologica
588 Sinica 21, 1281-1301.

589 Gu, H.O., Xiao, Y., Santosh, M., Li, W.Y., Yang, X., Pack, A.,Hou, Z., 2013. Spatial and temporal
590 distribution of Mesozoic adakitic rocks along the Tan-Lu fault, Eastern China: Constraints on the
591 initiation of lithospheric thinning. Lithos 177, 352-365.
592 Hacker, B., Ratschbacher, L., Webb, L., Ireland, T., Walker, D., Dong, S.W., 1998. U/Pb zircon ages
593 constrain the architecture of the ultrahigh-pressure Qinling-Dabie Orogen, China. Earth and Planetary
594 Science Letters 161, 215-230.
595 Hao, T. Y., Xu, Y., Suh, M., Liu, J. H., Zhang, L. L., Dai, M. G., 2007. East Marginal Fault of the Yellow
596 Sea: a part of the conjunction zone between Sino-Korea and Yangtze Blocks? Geological Society,
597 London, Special Publications 280, 281-291.
598 Zhang, K., K., Lü, Q., Yan, J., Hu, H., Fu, G., Shao, L., 2018. Crustal structure beneath the Jiaodong
599 Peninsula, North China: revealed with a 3D inversion model of magnetotelluric data: Journal of
600 Geophysics and Engineering 15, 2442.
601 Lai X.Y., 1997. Terrane collage and ultrahigh pressure metamorphism in Jiaodong (PhD thesis [in
602 Chinese with English abstract] Beijing, China University of Geosciences).
603 Li, H.Y., Xu, Y.G., Liu, Y.M., Huang, X.L., He, B., 2013. Detrital zircons reveal no Jurassic plateau in
604 the eastern North China Craton. Gondwana Research 24, 622-634.
605 Li, S., Jahn, B.-m., Zhao, S., Dai, L., Li, X., Suo, Y., Guo, L., Wang, Y., Liu, X., Lan, H., Zhou, Z., Zheng,
606 Q., Wang, P., 2017. Triassic southeastward subduction of North China Block to South China Block:
607 Insights from new geological, geophysical and geochemical data. Earth-Science Reviews 166, 270-
608 285.

609 Lin, W., Monié, P., Faure, M., Schärer, U., Shi, Y., Breton, N.L., Wang, Q., 2010. Cooling paths during
610 the Mesozoic extensional tectonics of NE China: example from the South Liaodong Peninsula
611 Metamorphic Core Complex. Journal of Asian Earth Sciences 42, 1048-1065.
612 Liu, F.L., Wang, F., Liu P.H., 2009a. Genetic relationship between pegmatite formation and Anatexis of
613 ultrahigh-pressure (UHP) metamorphic rocks in the Weihai Area, North Sulu UHP Terrane. Acta
614 Geologica Sinica 83, 1687-1702 (in Chinese with English abstract).
615 Liu, F.L., Xue, H.M., Liu, P.H., 2009b. Partial melting time of ultrahigh-pressure metamorphic rocks in
616 the Sulu UHP terrane: Constrained by zircon U-Pb ages, trace elements and Lu-Hf isotope
617 compositions of biotite-bearing granite. Acta Petrologica Sinica 25, 1039-1055.
618 Liu, J., Davis, G., Lin, Z., Wu, F., 2005. The Liaonan metamorphic core complex, Southeastern Liaoning
619 Province, North China: A likely contributor to Cretaceous rotation of Eastern Liaoning, Korea and
620 contiguous areas. Tectonophysics 407, 65-80.
621 Liu J.W., Yu Z.A., Mao Z.Y., 1994. Wendeng and Weihai map of mineral deposit of the People's Republic
622 of China (Map scale: 1:200000). Shandong Bureau of Geology and Mineral Resources (map materials,
623 in Chinese).
624 Liu, X., Deng, J., Liang, Y., Wang, Q., Pan, R., Qin, C., Yang, Y., 2018. Petrogenesis of Early Cretaceous
625 intermediate-felsic dikes in the Jiaodong Peninsula, south-eastern North China Craton: Constraints
626 from geochronology, geochemistry and Sr-Nd-Pb-Hf isotopes. Gondwana Research 60, 69–93.
627 Liu, Y. S., Hu, Z. C., Gao, S., Günther, D., Xu, J., Gao, C.G., Chen, H.H., 2008. In situ analysis of major
628 and trace elements of anhydrous minerals by LA-ICP-MS without applying an internal standard.
629 Chemical Geology 257, 34-43.

630 Maruyama, S., Isozaki, Y., Kimura, G., Terabayashi, M., 1997. Paleogeographic maps of the Japanese
631 Islands: Plate tectonic synthesis from 750 Ma to the present. Island Arc 6, 121-142.
632 Mattauer, M., Matte, P., Malavieille, J., Tapponnier, P., Maluski, H., Xu, Z., Lu, Y., Tang, Y., 1985.
633 Tectonics of the Qinling Belt: build-up and evolution of eastern Asia. Nature 317, 496-500.
634 Ni Z.Y., 1999. Formation, evolution and geological significance for the proterozoic ophiolite in Jiaodong
635 Peninsula (Ph. D. thesis [in Chinese with English abstract] Beijing, Peking University).
636 Oh, C. W., 2006. A new concept on tectonic correlation between Korea, China and Japan: Histories from
637 the late Proterozoic to Cretaceous. Gondwana Research 9, 47-61.
638 Oh, C. W., Kusky, T., 2007. The Late Permian to Triassic Hongseong-Odesan Collision Belt in South
639 Korea, and its tectonic correlation with China and Japan. International Geology Review 49, 636-657.
640 Oh, C. W., Choi, S. G., Seo, J., Rajesh, V. J., Lee, J. H., Zhai, M., Peng, P., 2009. Neoproterozoic tectonic
641 evolution of the Hongseong area, southwestern Gyeonggi Massif, South Korea; implication for the
642 tectonic evolution of Northeast Asia. Gondwana Research 16, 272-284.
643 Oh, C.W., Lee, B.C., 2018. The relationship between systematic metamorphic patterns and collisional
644 processes along the Qinling–Sulu–Odesan collisional belt between the North and South China
645 Cratons. Geological Society, London, Special Publications 478, https://doi.org/10.1144/SP478.5
646 Phillips, G.N., Powell, R., 2015. A practical classification of gold deposits, with a theoretical basis. Ore
647 Geology Reviews 65, 568-573.
648 Ratschbacher, L., Hacker, B., Calvert, A., Webb, L., Grimmer, J., McWilliams, M., Ireland, T., Dong, S.,
649 Hu, J., 2003. Tectonics of the Qinling (Central China): tectonostratigraphy, geochronology, and
650 deformation history. Tectonophysics 366, 1-53.

651 Seo, J., Choi, S.G., Oh, C.W., 2010. Petrology, geochemistry, and geochronology of the post-collisional
652 Triassic mangerite and syenite in the Gwangcheon area, Hongseong Belt, South Korea. Gondwana
653 Research 18, 479-496.
654 Shandong Bureau of Geology and Mineral Resources (SBGMR).1991. Regional Geology Part one No.
655 26, Regional geology of Shandong Province, Geological special report of the Ministry of Geology
656 and Mineral Resources of the People's Republic of China. Geological Publishing House, Beijing, pp.
657 1-595 (in Chinese).
658 SoeThura, T., Watkinson, I. M., 2017. The Sagaing Fault, Myanmar (Chapter 19). Geological Society
659 London Memoirs 48, 413-441.
660 Song M.C. and Miao P.C. 2003. Regional geology of Shandong Province. Shandong Map Publishing
661 House, Jinan, P.R. China, pp.1-968 (in Chinese).
662 Tang J., Zheng Y.F., Wu Y.B., Gong B., 2005. A study of zircon U-Pb dating and oxygen isotopes in UHP
663 granite gneiss from the Weihai Region in Northeast Sulu. Earth Sciences——Journal of China
664 University of Geosciences 30, 692-706.
665 Wan T.F., 2011. The Tectonics of China: Data, Maps and Evolution. Higher Education Press and Springer,
666 pp.1-506.
667 Wang, F., Zhu, R.X., Hou, Q.L., Zheng, D.W., Yang, L.K., Wu, L., Shi, W.B., Feng, H.L., Sang, H.Q.,
668 Zhang, H.Y., Liu, Q., 2014. 40Ar/39Ar Thermochronology on Central China Orogen: Cooling, uplift
669 and implications for orogeny dynamics. Geological Society London Special Publications 378, 189-
670 206.
671 Wang, R.M., An, J.T., Lai, X.Y., 1995. The discovery of an Ophiolite Suite in eastern part of Shandong
672 Peninsula and its significance. Acta petrologica sinica 11(suppl.), 221-227.

673 Wawrzenitz, N., Romer, R.L., Oberhänsli, R., Dong, S., 2006. Dating of subduction and differential
674 exhumation of UHP rocks from the Central Dabie Complex (E-China): Constraints from microfabrics,
675 Rb-Sr and U-Pb isotope systems. Lithos 89, 174-201.
676 Wiedenbeck M., Allé P., Corfu F., Griffin, W.L., Meier, M., Oberli, M., Oberli, F., Von Quadt, A., Roddick,
677 J.C., Spiegel, W., 1995. Three natural zircon standards for U-Th-Pb, Lu-Hf, trace element and REE
678 analysis. Geostandards Newsletter 19, 1-23.
679 Wiedenbeck M., Hanchar J. M., Peck W. H., et al., 2004. Further characterisation of the 91500 zircon
680 crystal. Geostandards and Geoanalytical Research 28, 9-39.
681 Wu, L., Monié, P., Wang, F., Lin, W., Ji, W., Yang, L., 2017. Multi-phase cooling of Early Cretaceous
682 granites on the Jiaodong Peninsula, East China: Evidence from 40Ar/39Ar and (U-Th)/He
683 thermochronology. Journal of Asian Earth Sciences 160, 334-347.
684 Wu, Y.B., Zheng, Y.F., 2004. Genesis of zircon and its constraints on interpretation of U-Pb age. Chinese
685 Science Bulletin 49, 1554-1569.
686 Xiao Q.B., 2008. Electrical structure study of the crust-upper mantle in Dabie-Sulu orogen (Postdoctoral
687 report [in Chinese] Beijing, China Earthquake Administration).
688 Xu, P., Liu, F., Ye, K., Wang, Q., Cong, B., Chen, H., 2002. Flake tectonics in the Sulu orogen in eastern
689 China as revealed by seismic tomography. Geophysical Research Letters 29 (10), 1385.
690 Xu, Y.G., 2006.Diachronous lithospheric thinning of the North China Craton and formation of the
691 Daxin'anling–Taihangshan gravity lineament. Lithos 96, 281-298.
692 Yan, Q., Metcalfe, I., Shi, X., Zhang, P., Li, F., 2018. Early cretaceous granitic rocks from the southern
693 Jiaodong Peninsula, eastern China: implications for lithospheric extension. International Geology
694 Review 61, 821-838.

695 Yang, J.H., Chung S.L., Wilde, S.， Wu, F.Y., Chu, M.F., Lo, C.H.， Fan, H.R., 2005. Petrogenesis of
696 post-orogenic syenites in the Sulu Orogenic Belt, East China: geochronological, geochemical and
697 Nd-Sr isotopic evidence. Chemical Geology 214, 99-125.
698 Yang, J.H., Wu, F., 2009. Triassic magmatism and its relation to decratonization in the eastern North
699 China Craton. Science in China Series D: Earth Sciences 52, 1319-1330.
700 Yang J.S., Xu Z.Q., Wu C.L., Liu F.L., Shi R.D., Wooden J., Maruyama S., 2002. SHRIMP U-Pb Dating
701 on Coesite-Bearing Zircon: Evidence for Indosinian Ultrahigh-Pressure Metamorphism in Su-Lu，
702 East China. Acta Geologica Sinica 76, 354-372 (in Chinese with English abstract).
703 Yang J.S., Liu F.L., Wu C.L., Wan Y.S., Zhang J.X., Shi R.D., Chen S.Y., 2003. Two Ultrahigh Pressure
704 Metamorphic Events Recognized in the Central Orogenic Belt of China: Evidence from the U-Pb
705 Dating of Coesite-bearing Zircons. Acta Geologica Sinica 77, 463-477 (in Chinese with English
706 abstract).
707 Yang J.S., Xu Z.Q., Zhang J.X., Zhang Z.M., Liu F.L., Wu C.L., 2009. Tectonic setting of main high-and
708 ultrahigh-pressure metamorphic belts in China and adjacent region and discussion on their subduction
709 and exhumation mechanism. Acta Petrologica Sinica 25, 1529-1560 (in Chinese with English
710 abstract).
711 Yang L.Q., Deng J., Goldfarb R.J., Zhang J., Gao B.F., and Wang Z.L., 2014. 40Ar/39Ar
712 geochronological constraints on the formation of the Dayingezhuang gold deposit: new implications
713 for timing and duration of hydrothermal activity in the Jiaodong gold province, China. Gondwana
714 Research 25, 1469-1483.
715 Yang, Y.S., Li, Y.-y., 2018. Crustal structure of the Dabie orogenic belt (eastern China) inferred from
716 gravity and magnetic data. Tectonophysics 723, 190-200.

717 Ye K., Cong B.L., 1995. Petrological study of UHP metamorphic silicate rocks from Tengjiaji,
718 Rongcheng County. Chinese Science Bulletin 40, 730-733 (in Chinese).
719 Ye, K., Cong, B., Ye, D., 2000. The possible subduction of continental material to depths greater than
720 200 km. Nature 407, 734-736.
721 Ye, K., Song, Y. R., Chen, Y., Xu, H. J., Liu, J. B., Sun, M., 2009. Multistage metamorphism of orogenic
722 garnet–lherzolite from Zhimafang, Sulu UHP terrane, E. China: Implications for mantle wedge
723 convection during progressive oceanic and continental subduction. Lithos 109, 155-175.
724 Yutaka, T., Deung-Lyong, C., Jianren, M., Xilin, Z., Keewook, Y., 2018. SHRIMP U–Pb zircon ages of
725 the Hida metamorphic and plutonic rocks, Japan: Implications for late Paleozoic to Mesozoic
726 tectonics around the Korean Peninsula. Island Arc 27, e12220.
727 Zhao, Z.F., Liu, Z.-B., Chen, Q., 2017. Melting of subducted continental crust: Geochemical evidence
728 from Mesozoic granitoids in the Dabie-Sulu orogenic belt, east-central China. Journal of Asian Earth
729 Sciences 145, 260-277.
730 Zhang, R.Y., Liou, J.G., Ernst, W.G., 2009. The Dabie–Sulu continental collision zone: A comprehensive
731 review. Gondwana Research 16, 1-26.
732 Zhang, H.F., Sun, M., 2002. Geochemistry of Mesozoic basalts and mafic dikes, southeastern North
733 China Craton, and tectonic implications. International Geology Review 44, 370-382.
734 Zhang H.Y., 2003. The Research on Mesozoic Thrust-Nappe Structure in Eastern Jiaodong (Shandong
735 Province, China [Master degree thesis, in Chinese with English abstract] Beijing, China University
736 of Mining and Technology).
737 Zhang, H.Y., Hou,Q., Cao, D., 2005. Ultramicrostructure research of the Mesozoic slip-thrust belt in the
738 eastern of Jiaodong peninsula. Geology of China 32, 571-578 (in Chinese with English abstract).

739 Zhang, H.Y., Hou,Q., Cao, D., 2007a. Study of thrust and nappe tectonics in the Eastern Jiaodong
740 peninsula, China. Science in China, Series D 50, 161-171.
741 Zhang, H.Y., Hou,Q., Cao, D., 2007b. Tectono-chronologic constraints on a Mesozoic slip and thrust belt
742 in the Eastern Jiaodong peninsula. Science in China, Series D 50, 25-32.
743 Zhang, L., Yang, L.Q., Weinberg, R.F., Groves, D.I., Wang, Z.L., Li, G.W., Liu, Y., Zhang, C., Wang,
744 Z.K., 2019. Anatomy of a world-class epizonal orogenic-gold system: A holistic thermochronological
745 analysis of the Xincheng gold deposit, Jiaodong Peninsula, eastern China. Gondwana Research 70,
746 50–70.
747 Zhang, W. Y. (ed.), 1986. Marine and Continental Tectonics in China Seas and Adjacent Regions
748 (1:5,000,000). Science Press, Beijing, pp.162–177 (in Chinese).
749 Zhang, X.J., Zhang, W., Fan, Z.L., Zhu, W.P. Tong, J., Yao, G.T., 2017a. Characteristics of airborne
750 gravity field and the main geological discovery in the northern South Yellow Sea. Geological Survey
751 of China 4, 50-56 (in Chinese with English abstract).
752 Zhang, X.J., Zhang, W., Tong, J., Fan Z.L., Li X., 2017b. Magnetic and gravity anomaly characteristics
753 of main faults in Rizhao-Lianyungang area. Geological Survey of China 4(Issue 6), 66-70 (in Chinese
754 with English abstract).
755 Zheng, Y.F., Zhou, J.B., Wu, Y.B.,Xie, Z., 2005. Low-grade metamorphic rocks in the Dabie-Sulu
756 orogenic belt: A passive-margin accretionary wedge deformed during continent subduction.
757 International Geology Review 47, 851-871.
758 Zhu G., Xu J.W., 1994. Deformation and metamorphic evolution in the Jiaobei Region, Eastern
759 Shandong.
760

761 **Table 1 Triassic isotopic dating results of granitic and high pressure metamorphic rocks by**
762 **former authors**

Settings	Location	Zircon types	Rock types	Ages （Ma)	Measuring Methods	Data references
II-2-①	Jiazishan	Magmatic	quartz-syenite	215±5	SHRIMP Zircon U-Pb	Yang et al, 2005
			Quartz-syenite	219.7±2.1	Single grain zircon isotope dilution	Chen et al, 2003
			Pyroxene syenite	225.3±1.9	Single grain zircon isotope dilution	Chen et al, 2003
			Pyroxene syenite	209.0±6.5	Single grain zircon isotope dilution	Guo et al., 2005
			Pyroxene syenite	211.9±1.5	Single grain zircon isotope dilution	Guo et al., 2005
	Xingjia	Magmatic	Alkaline gabbro	213±5	SHRIMP Zircon U-Pb	Guo et al., 2005
			Alkaline gabbro	211±5	SHRIMP Zircon U-Pb	Guo et al., 2005
			Syenogranite	205±5	Single grain zircon isotope dilution	Chen et al, 2003
	Chashan, Rongcheng	Magmatic	Syenogranite	222.1±1.6	Single grain zircon isotope dilution	Chen et al, 2003
			Syenogranite	205.7±1.4	Single grain zircon isotope dilution	Guo et al., 2005
	Renheji	Magmatic	Quartz-syenite	211.0±0.9	Single grain zircon isotope dilution	Chen et al, 2003
	Datuan, Rongcheng	Metamorphic ring	Eclogite	228±29	SHRIMP Zircon U-Pb	Yang et al.,2002
II-1	Zaobu, Weihai	Magmatic	Granitic gneiss	232±4	SHRIMP Zircon U-Pb	Tang et al.,2005
	Wenquan, Weihai	Metamorphic ring	Ultramafic rock	221±12	SHRIMP Zircon U-Pb	Yang et al.,2002

I	Xiaoshidao, Weihai	Magmatic	Biotite granite	215.7±1.8	Single grain zircon isotope dilution	Liu et al.,2009a
	Sunjiatong, Weihai	Magmatic	Pegmatite	225±20	Zircon LA-ICP-MS	

763

764 Journal of Hefei University of Technology 17, 148-162 (in Chinese with English abstract).

765

766

767 **Table 2 Sample dating results of zircon U-Pb LA-ICP-MS in this paper**

Sample code	Rock types	Results /Ma	Coordinates	Occurrence	Tectonic significance
131102	Dolerite	210.5±1.0	N37°23′42.76″ E122°39′39.96″	Dyke in CSTG, Luofenggang	Syn-post-orogenic extension, about 220-210Ma
140304	granite	216.2±2.4	N36°56′09.92″ E122°27′15.23″	Dyke in SDG, Chishan	
140203	Gabbro	244.7±4.2	N37°07′40.62″ E122°21′24.71″	Sill, Donglinghou	Minimum time of orogenic related regional thrust and nappe system, about 240Ma.
140302	Gneissic granite	233.8±8.1	N37°09′56.96″ E122°34′18.434″	Sill, Qingyutan	

768

769

Table 4 relations of collisional zones in Eastern Asia

Settings		Jiaodong (This paper)	Western coastal region of Korea Peninsular (after Yutaka et al., 2018)	Hida Belt of Japan (after Yutaka et al., 2018)
Jurassic	Strike-slip event	Linglong Granite (Foliated) Wendeng Granite (WDG)	Sunchang Granite (Foliated)	-
		Dashijia shear zone (DSSZ)	**Cheongsan ductile shear zone**	**Mylonitization of the Hida younger granite**
Late Triassic	**Extension event**	**Chengshantou Granite** **Shidao Granite**	**Boeun Granite**	**Okumayama granodiorite (Hida younger granite)**
		Upper Jiashan-Xiangshui Detachment (U-JSXS)	-	**Mylonitization of the Hida older granite**
Early-Middle Triassic	**Collision event**	**Donglinghou gabbro sill** **Qingyutan granite sill**	**Cheongsan Granite**	**Hida older granite**
		UHP-wedge (Jiaonan Group)	**Ogcheon metamorphic rocks**	**Hida metamorphic rocks**

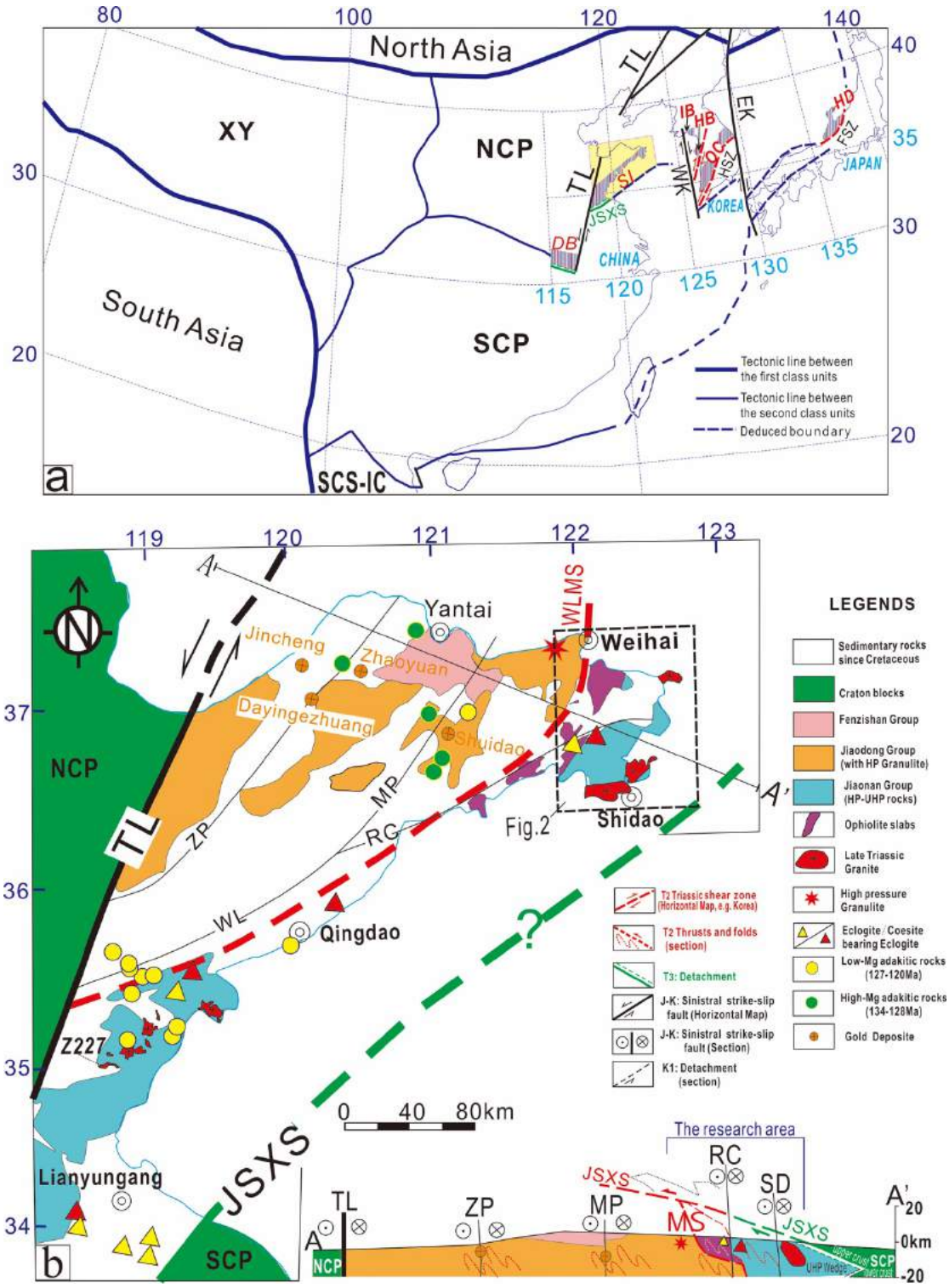

778

779 **Fig. 1 Tectonic background of the Jiaodong research area**

780 a- Eastern Asian Tectonics along the collision belt between the North China and the South China plates in Triassic

781 (revised after Ge & Ma, 2014 and Yutaka et al., 2018). **The second class units:** XY-Xiyu Plate; SCS-IC-South China

782 Sea and IndoChina Plate; NCP-North China Plate; SCP-South China Plate. **Tectonic zones:** DB-the Dabie Belt; SL-
783 the Su-Lu Belt; IB-the Imjingang Belt; HB-the Hongsung Belt; OC- the Ogcheon Belt; HD- the Hida Belt; JSXS-
784 the Jiashan-Xiangshui Shear Zone; HSZ-the Honam Shear Zone; FSZ-the Funatsu Shear Zone; TL-the Tancheng-
785 Lujiang Fault Zone; WK-the Western Coastal Fault Zone of Korea; EK- the Eastern Coastal Fault Zone of Korea.

786 b- **Triassic regional outline map of the Su-Lu Belt. T_2 thrust and folding: WLMS-the Wulian-Mishan shear**
787 **zone**; **middle to late Triassic detachment:** JSXS. **J-K strike-slip faults/ shear zones:** ZP-the Zhaoyuan-Pingdu
788 Fault; MP-the Muping Fault; RC-the Rongcheng Fault; WL-the Wulian Fault. Eclogite/coesite bearing locations are
789 after Ye K. et al.(1995). High pressure granulite location is according to Wang et al.(1995). Exposed locations of
790 Early Cretaceous adakitic rocks are after Gu et al. (2013). **Section A-A'** demonstrates space-time relations of shear
791 zones and featured rock types, in which the crocodile geometry of the SCP is after the Cross-P-velocity section
792 across the Jiaodong Peninsula by Xu et al. (2002). Since the Shidao Fault (SD) and the Muping Fault (MP) have
793 similar sinistral shearing sense, here we consider the Jiashan-Xiangshui fault zone (JSXS) as the boundary between
794 the NCP and SCP, which is different from the consideration of Xu et al. (2002).

795

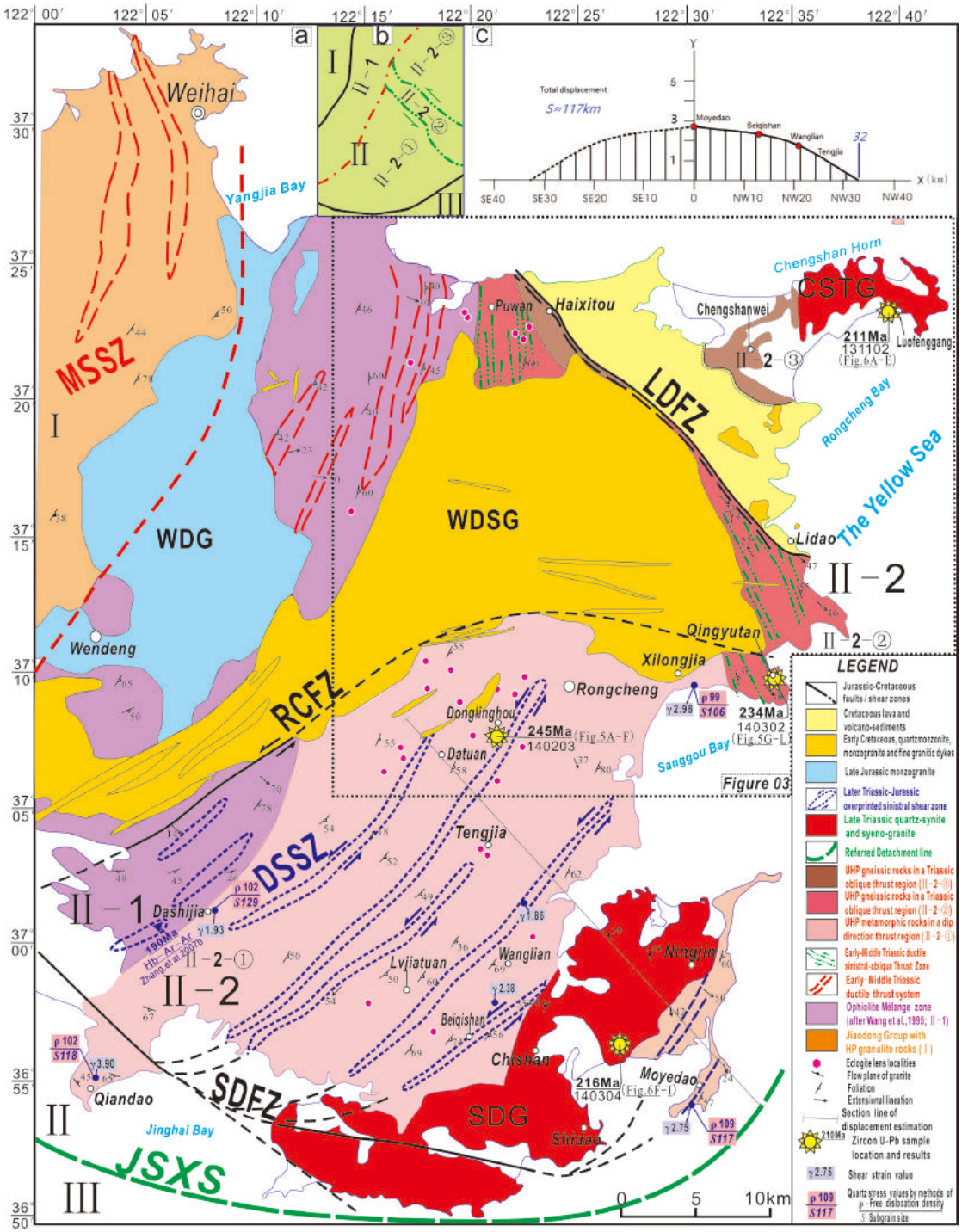

Fig.2 Structural map of the research region

(a) Structural map: **Granitoids:** SDG-the Shidao granitoid; CSTG- the Chengshantou granitoid; WDG-the Wendeng granitoid; WDSG-the Weideshan granitoid. **Syncollisional shear zone:** MSSZ-the Mishan Shear Zone; **Postcollisional extension:** JSXS - the Jiashan-Xiangshui Detachment; **Jurassic overprinted shear zone:** DSSZ-the Dashijia Shear Zone; **Jurassic-Cretaceous**

fault zone: RCFZ-the Rongcheng Fault Zone; SDFZ-the Shidao Fault Zone; LDFZ-the Lidao Fault Zone**.**

(b) Sketch map on tectonic division: I-Jiaodong Group, the lower crust unit of the NCP. II-Triassic orogenic complex: II-1 the ophiolite mélange unit; II-2 the eclogite-rich unit: II-2 -① is a Triassic thrust zone superposed by Jurassic sinistral strike slip shearing, II-2 -② is a Triassic sinistral-oblique thrust zone and II-2 -③ is a Triassic thrust zone; III-SCP. **(c) Displacement estimation section in unit II-2 -①**. Regions of Figs.3-6 are also shown in this figure.

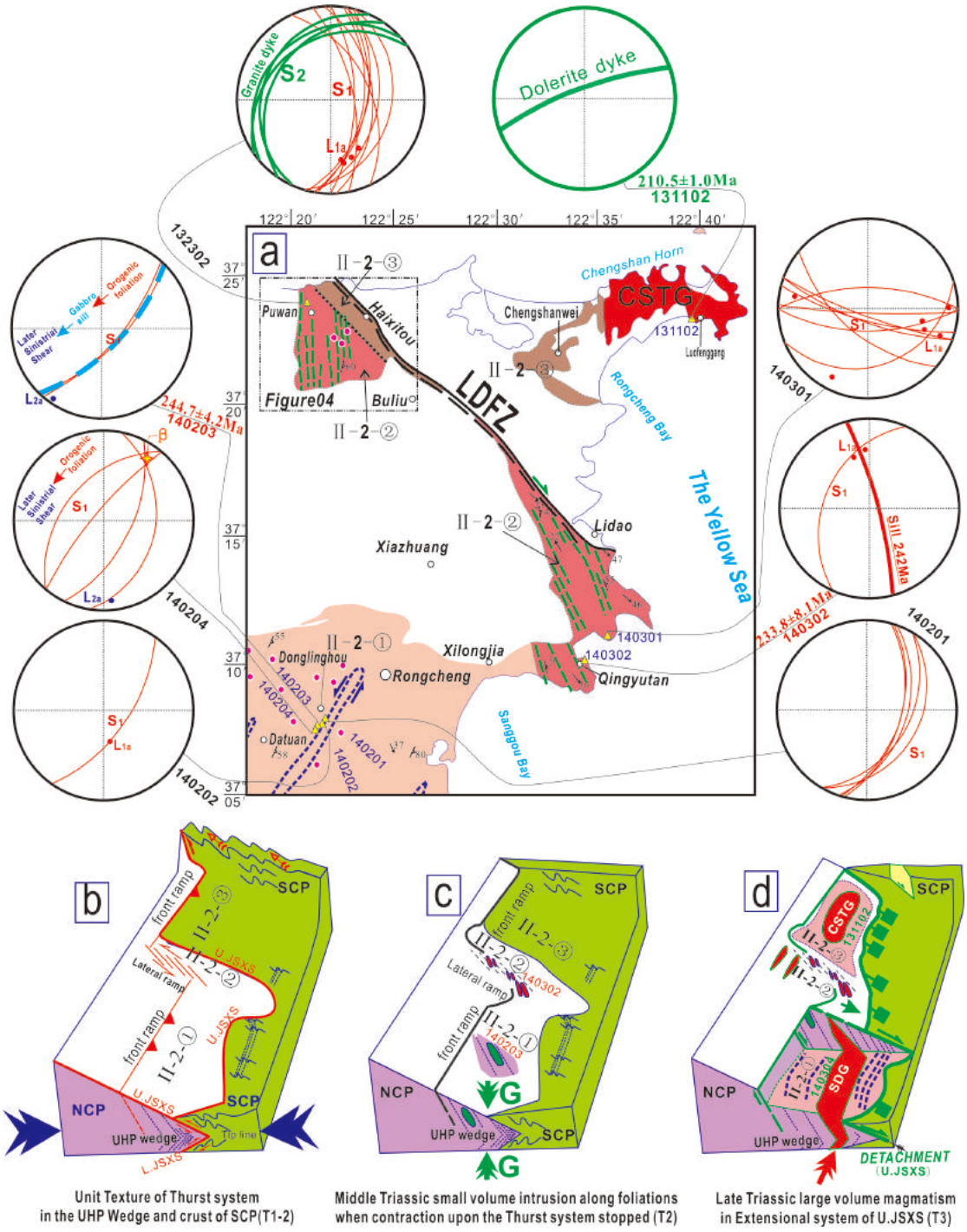

807

808 **Fig.3 Superposed structural elements in the research region (Base map is after Liu et al., 1994)**

809 (a) Tectonic outline map with structural elements; (b-d) Evolution stages of syncollisional thrust

810 system and sampling background. Note： In (b), red lines demonstrate a thrust system, while blue

811 arrows show contraction direction and dashed blue lines represent foliations inside the UHP wedge;

In (c), G and green arrows show force direction of gravity; In (d), green lines demonstrate the detachment system, while red arrow indicates the magma route. Here, x and y axes represent W-E from left to right and N-S from upper to below respectively.

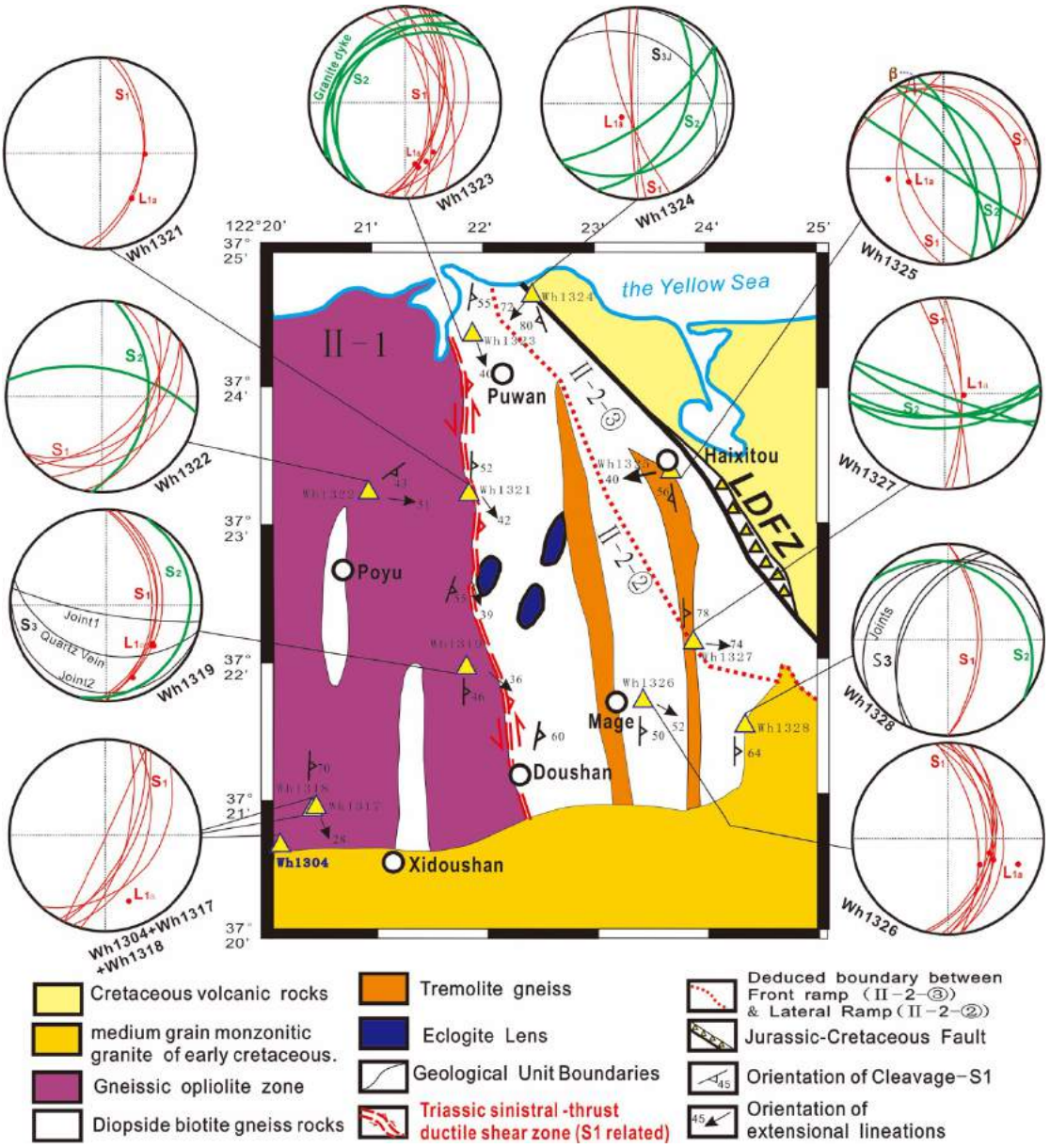

816

817 **Fig.4 Superposed structural elements in the Puwan region, the north part of unit II-2 -②**

818 **(Base map is after Liu et al.,1994)**

819 The boundary of gneissic ophiolite zone (II-1) with NW part of the UHP belt (II-2-②) is a sinistral thrust ductile

820 shear zone which becomes broader in the Doushan-Mage area. The stereoplots indicate different stages of

821 structural elements. Foliations and lineations of the first stage caused by the contractional event during Orogenism

822 are plotted in red as S_1 and L_{1a}, respectively. In localities 1319, 1321, 1323 and 1326, there are quite similar

823 orientations of structural elements in the first stage indicating sinistral strike slip but top to NW thrusting

movement. In localities1324, 1325 and 1327, there are mainly frontal ramp style thrusts with superposed folding. Therefore, the unit II-2-② (the lateral ramp unit) and the unit II-2-③ (the front ramp unit) can be divided by the red dotted line according to their different relations between S_1 and L_{1a}. Basic or granitic dykes, or veins shown in green color were formed during the Late Triassic extension. Brittle joints and quartz veins were superposed later and are shown in black color. In the unit II-2-③, locality Wh1325 near Haixitou is unique because of an antiform fold happened. The surface orientations are projected into a β style diagram indicating that the antiform hinge line is plunging to NNW. Here, x and y axes represent W-E from left to right and N-S from upper to below respectively.

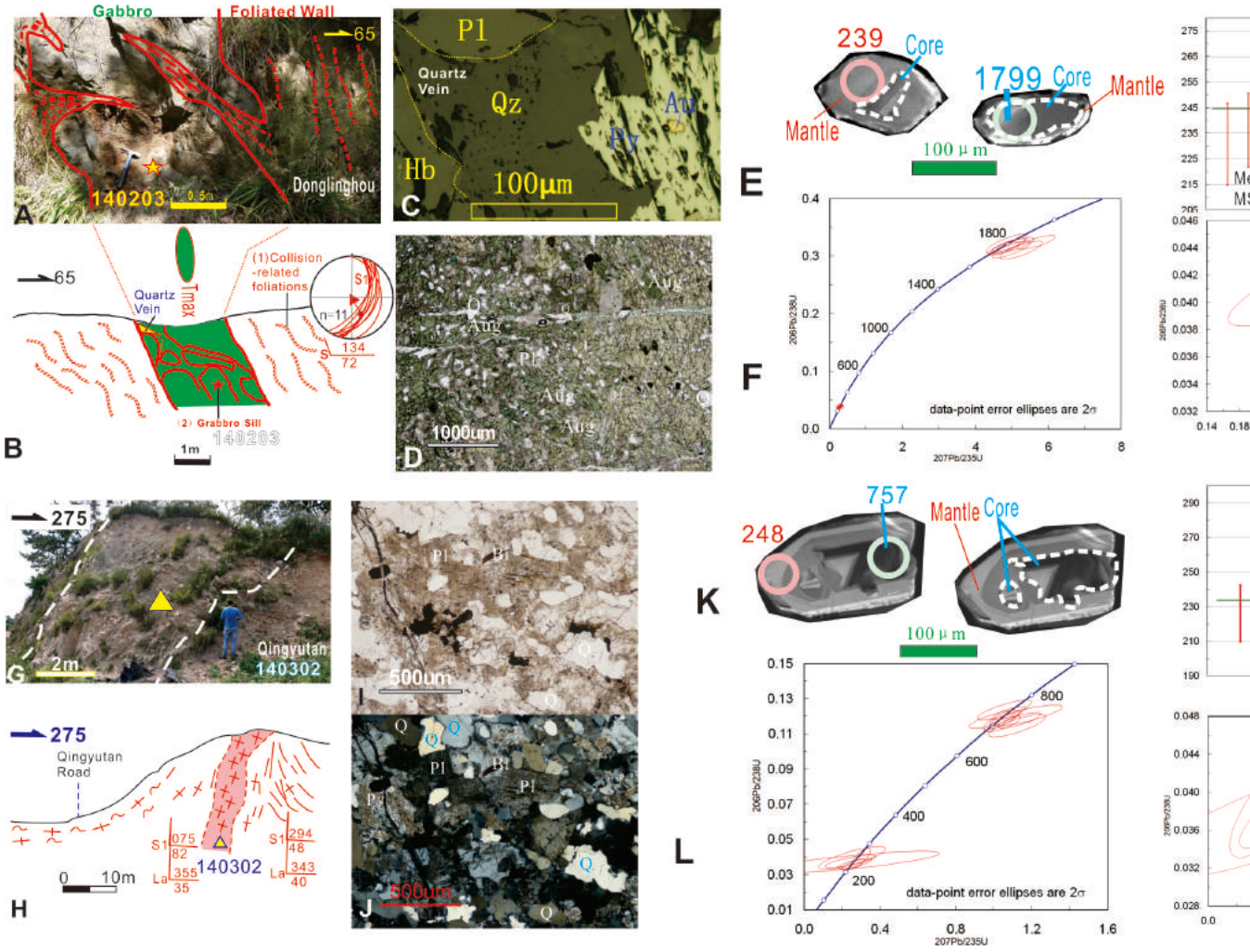

833

834 **Fig.5 Typical synthrusting intrusions and their features**

835 **A-F: Sample 140203 of gabbro sill intruded in gneissic host rocks, Donglinghou, NE side of Datuan Town**. A,

836 B- sample outcrop and sketch, foliated collision-related host and the intruded gabbroic sill; C- microphotograph of

837 gold bearing quartz vein; D- microphotograph; E- zircon features; F- U-Pb concordia and weighted average diagrams.

838 **G-L Sample 140302 from granitic sill intruded in genissic host rocks at Qingyutan.** G, H- sample outcrop and

839 sketch; I, J- microphotograph; K-zircon features； L- U-Pb concordia and weighted average diagrams. **Localities of**

840 **these two samples are shown in Fig.2.**

841

842

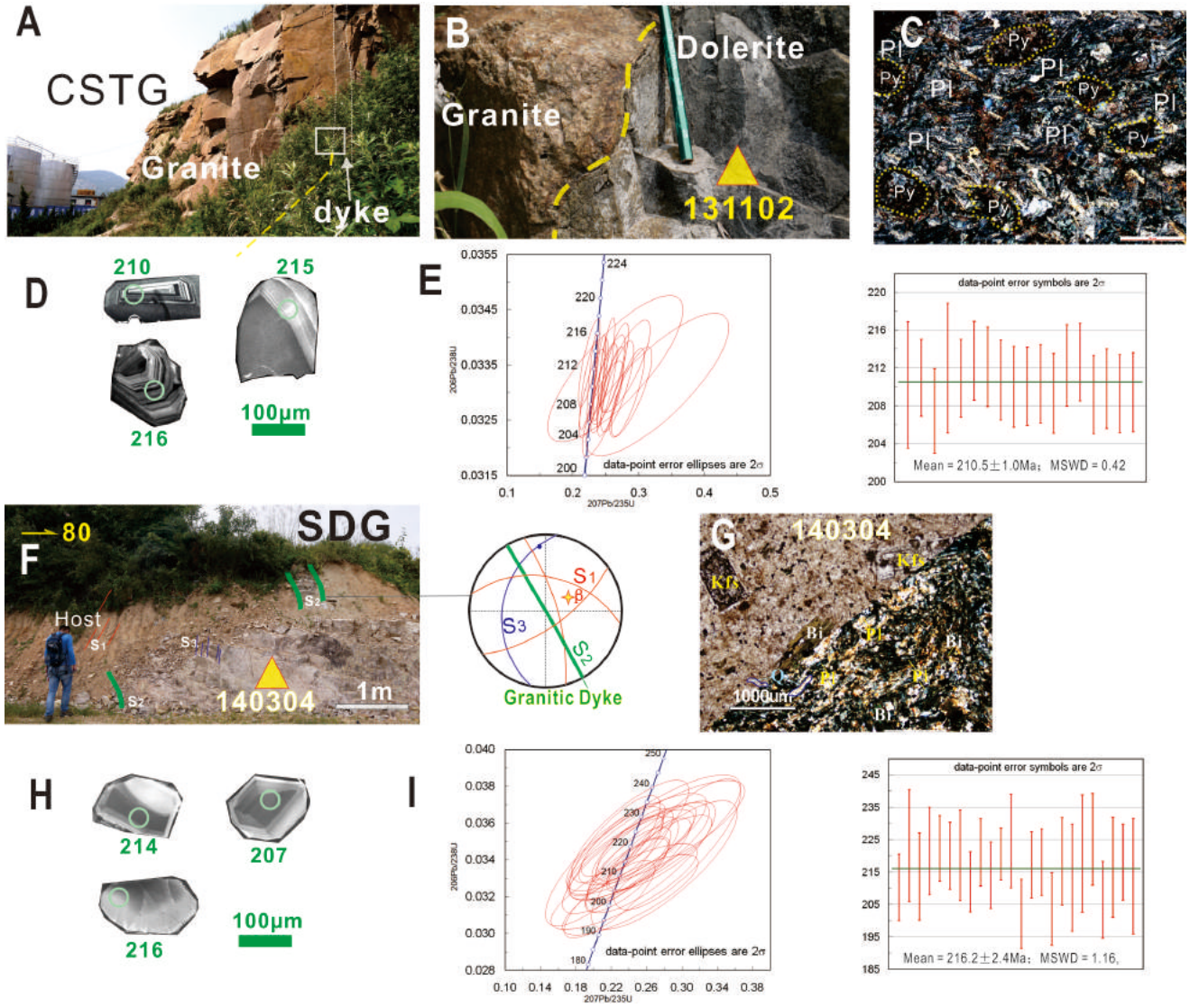

Fig.6 Typical postcollisional extension structures, intrusions and zircon features

A-E: 131102 from dolerite dyke intruded in granitoid, Luofenggang Village, Chengshantou. A, B- sample outcrops; C- microphotograph showing less deformed major minerals such as pyroxene (Py) and plagioclase (Pl); D- zircon features; E- U-Pb concordia and weighted average diagrams. **F-I: 140304 from thick granitic dyke, SE side of Chishan Town.** F- sample outcrops; G- microphotograph showing less deformed major minerals including K-feldspar (Kfs), plagioclase (Pl), Quartz (Q), biotite (Bi); H- zircon features; I- U-Pb concordia and weighted average diagrams. **Localities of these two samples can be found in Fig.2.**

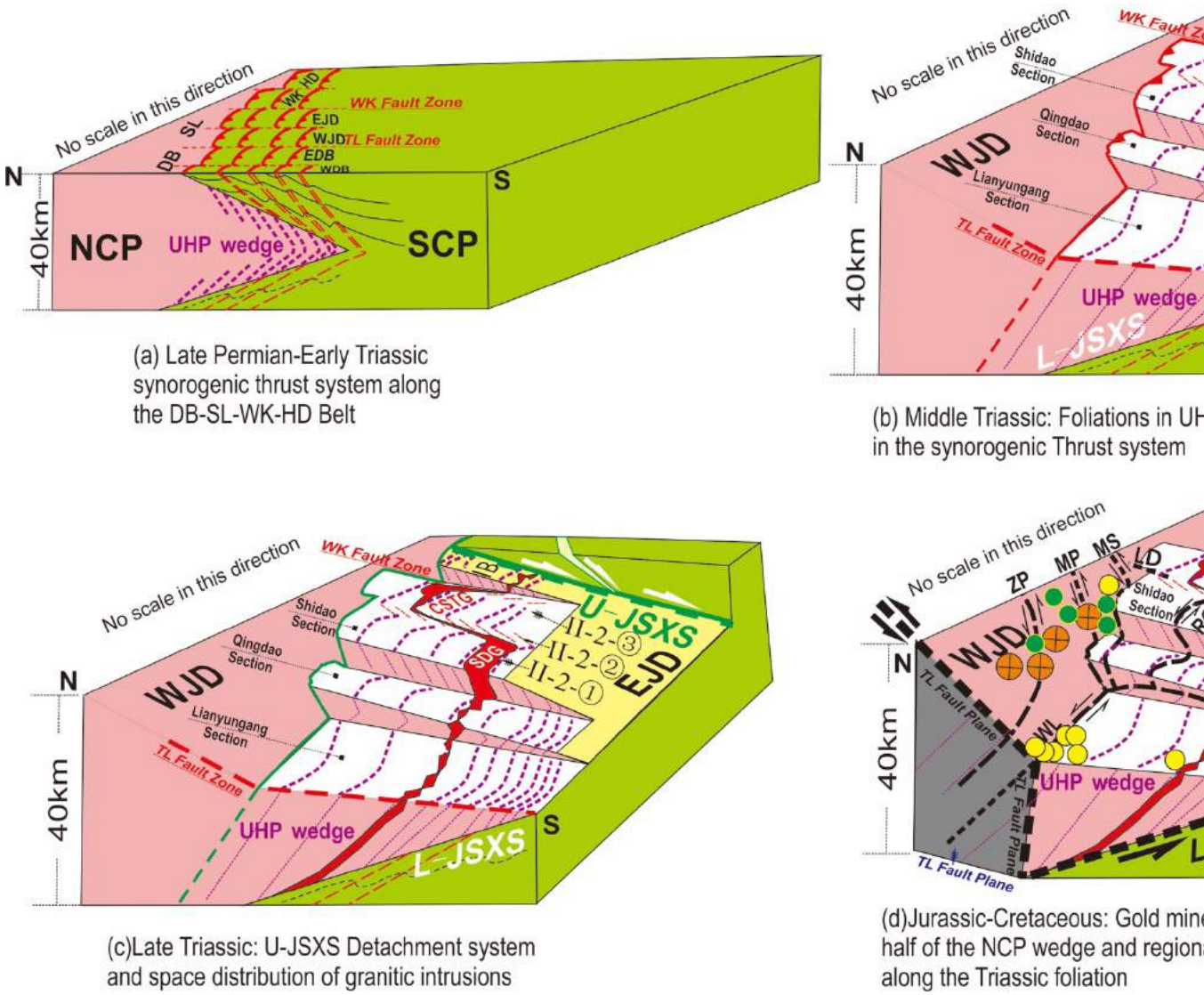

Fig. 7 3D Mesozoic evolution model of the UHP wedge in Jiaodong Peninsular

Codes notation: EJD-Eastern Jiaodong; WJD-Western Jiaodong; EDB-eastern Dabie Orogen; WDB -western Dabie Orogen; WK-Western Korean Belt (including IB, HB, OC); HD- the Hida Belt in Jappan; UHP wedge- ultrahigh pressure metamorphic wedge; L.SCP-Lower crust of the South China Plate; S.SCP-Upper crust of the South China Plate. **Triassic granitoids:** SDG-Shidao Granitoid; CSTG-Chengshantou Granitoid. **Jurassic granitoids:** WDG-Wendeng Granitoid; LLG-Linglong Granitoid. **Cretaceous granitoids:** RCG- Rongcheng Granite; GJLG-Guojialing Granitoid. **Shear zones or faults:** Red dashed lines-syncollisional thrust system; Dark green dashed line-Postcollisional U.JSXS detachment; Fresh green dashed line-Jurassic-Cretaceous L.JSXS detachment; Black lines-

the Tan-Lu Fault System (TL): ZP-Zhaoyuan-Pingdu Fault; MP-Muping Fault; MS-Mishan Fault; RC-Rongcheng Fault; LD-Lidao Fault; WL-Wulian ductile shear zone. Locations of gold deposits and adakitic rocks are plotted according to Fig.1.

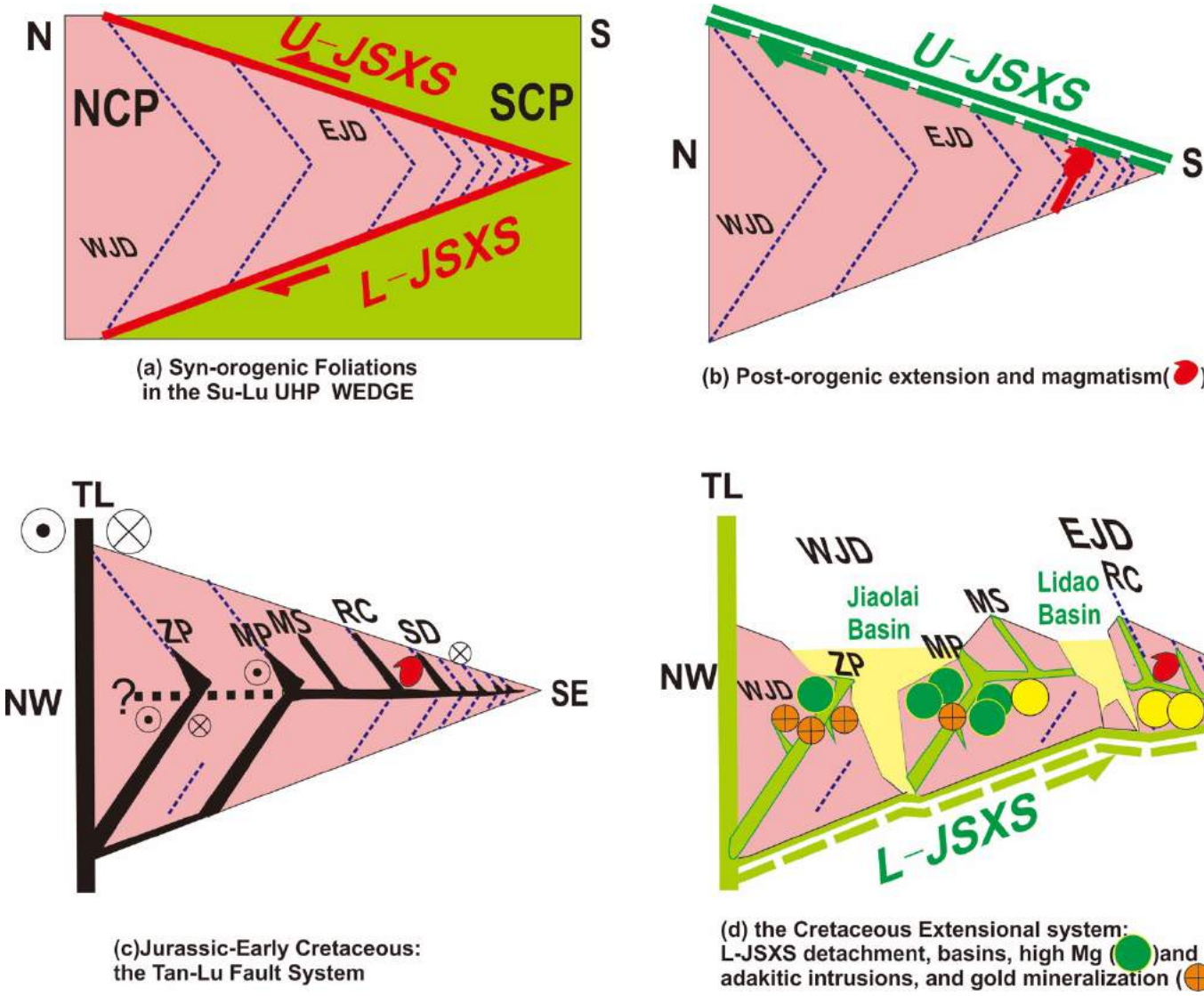

865

866 **Fig.8 Simplified 2D Mesozoic evolution model of the UHP wedge**

867 (a) is simplified from Fig.7a-b, indicating one contractional UHP wedge. Dashed lines in purple

868 means syncollisional foliations in the D1 stage when collision occurred between the NCP and SCP

869 along U-JSXS and L-JSXS reverse shear zones in red. (b) is after Fig.7c, showing intrusions below the

870 U-JSXS detachment in dark green. This is the D2 stage. (c-d) are divided from Fig.7d. (c) clarifies a

871 simplified Tan-Lu Fault system including major sinistral strike-slip faults since Jurassic. Dark lines

872 with title abbreviations refer to major regional faults. ZP-Zhaoping Fault; MP-Muping Fault; MS-

873 Mishan Fault; RC-Rongcheng Fault; SD-Shidao Fault. This is the early stage of D3 showing sinistral

shearing in an oblique contraction environment. (d) is the Cretaceous extensional system which indicates that gold mineralization and intrusion of adakitic rocks might have been confined by the middle plane of the tectonic wedge. The regional faults from the Tan-Lu fault system in fresh green are all thought to show an extensional nature. It is a later stage of D3. The Jiaolai Basin and Lidao Basin are both top basins of the L-JSXS detachment.